Cell Reports

Article

Brain connectivity inversely scales with developmental temperature in *Drosophila*

Graphical abstract

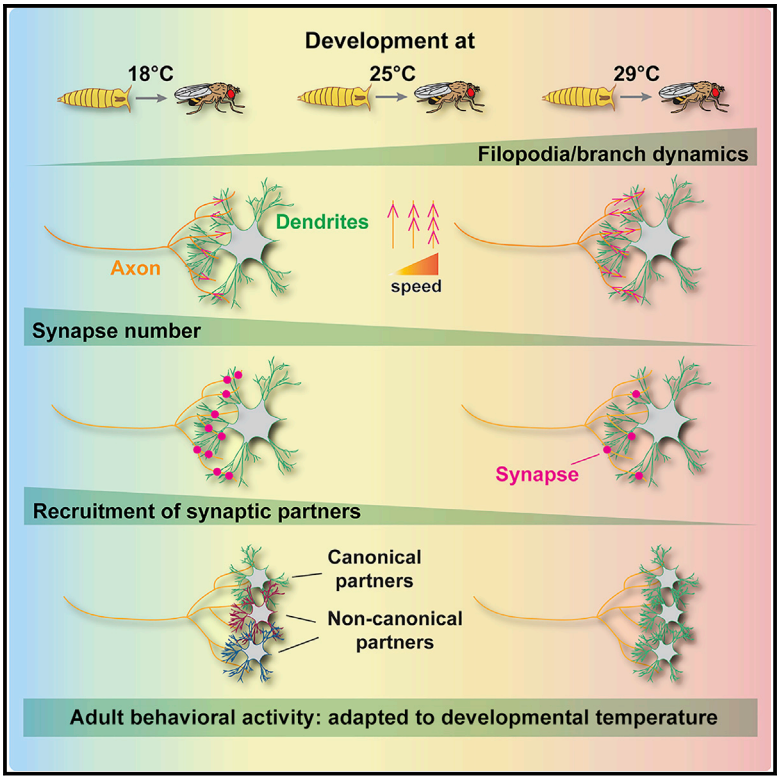

Highlights

- Developmental temperature affects synapse numbers and partner availability in flies
- Development at 18°C results in synaptic partnerships absent at 25°C
- The same non-canonical synapses form at 18°C and in the absence of a main partner at 25°C
- Adult behavioral activity is adapted for the temperature at which the fly developed

Authors

Ferdi Ridvan Kiral, Suchetana B. Dutta, Gerit Arne Linneweber, ..., Max von Kleist, Bassem A. Hassan, P. Robin Hiesinger

Correspondence

robin.hiesinger@fu-berlin.de

In brief

Different developmental temperatures lead to differently wired brains and behavioral adaptation to the temperature at which a fly developed. Kiral et al. propose that evolution has selected for a *Drosophila* genome that can develop functional, but non-identical, brains through scalable synapse formation based on relative availability of synaptic partners.

Kiral et al., 2021, Cell Reports *37*, 110145
December 21, 2021
https://doi.org/10.1016/j.celrep.2021.110145

CellPress

Cell Reports

CellPress
OPEN ACCESS

Article

Brain connectivity inversely scales with developmental temperature in *Drosophila*

Ferdi Ridvan Kiral,[1,5] Suchetana B. Dutta,[1] Gerit Arne Linneweber,[1] Selina Hilgert,[3] Caroline Poppa,[1] Carsten Duch,[3] Max von Kleist,[2] Bassem A. Hassan,[1,4] and P. Robin Hiesinger[1,6,*]

[1]Division of Neurobiology, Institute for Biology, Freie Universität Berlin, 14195 Berlin, Germany
[2]MF1 Bioinformatics, Robert Koch-Institute, 13353 Berlin, Germany
[3]Institute of Developmental Biology and Neurobiology (iDN), Hanns-Dieter-Hüsch-Weg 15, 55128 Mainz, Germany
[4]Institut du Cerveau – Paris Brain Institute – ICM, Sorbonne Université, Inserm, CNRS, Hôpital Pitié-Salpêtrière, Paris, France
[5]Present address: Department of Genetics, Yale Stem Cell Center, Yale School of Medicine, New Haven, CT 06520, USA
[6]Lead contact
*Correspondence: robin.hiesinger@fu-berlin.de
https://doi.org/10.1016/j.celrep.2021.110145

SUMMARY

Variability of synapse numbers and partners despite identical genes reveals the limits of genetic determinism. Here, we use developmental temperature as a non-genetic perturbation to study variability of brain wiring and behavior in *Drosophila*. Unexpectedly, slower development at lower temperatures increases axo-dendritic branching, synapse numbers, and non-canonical synaptic partnerships of various neurons, while maintaining robust ratios of canonical synapses. Using R7 photoreceptors as a model, we show that changing the relative availability of synaptic partners using a DIPγ mutant that ablates R7's preferred partner leads to temperature-dependent recruitment of non-canonical partners to reach normal synapse numbers. Hence, R7 synaptic specificity is not absolute but based on the relative availability of postsynaptic partners and presynaptic control of synapse numbers. Behaviorally, movement precision is temperature robust, while movement activity is optimized for the developmentally encountered temperature. These findings suggest genetically encoded relative and scalable synapse formation to develop functional, but not identical, brains and behaviors.

INTRODUCTION

In genetically identical organisms, brain wiring is not only precise but also flexible, robust to perturbation, and variable within limits (Goodman, 1978; Hiesinger and Hassan, 2018; Linneweber et al., 2020). Non-genetic perturbation can therefore reveal the limits of genetic determinism when combined with a quantitative description of precision versus variability. A non-genetic perturbation that affects all developmental processes is temperature (Gilbert, 2012; Gillooly et al., 2002). However, the extent to which developmental temperature changes synapse-specific connectivity of neural circuits is largely unknown.

Animals have adopted one of two evolutionary strategies to ensure functional outcomes: either to precisely control the developmental temperature (e.g., mammals, bee hives) or to evolve a developmental process that is robust to a certain temperature range (e.g., fish, flies). *Drosophila melanogaster* develops functional brains at temperatures between ~15°C and ~29°C, albeit with a more than 2-fold difference of developmental tempo (Kohrs et al., 2021). Temperature strictly determines molecular kinetics apparent as Brownian motion. However, the extent to which subcellular dynamics, synapse formation, and precise neural circuit formation change as a consequence of these molecular kinetic changes is, to our knowledge, not known for any neuron inside a developing brain.

Increasing temperature increases the pace of development in ectotherms such as amphibians and arthropods (Hertwig, 1898; Kuntz and Eisen, 2014; Zuo et al., 2012). Many neuron-based processes are unaffected by different temperatures (within a certain range) at the level of development or function, for example, the precision of circadian clocks (Kidd et al., 2015) and other rhythmic circuits (Alonso and Marder, 2020; Kushinsky et al., 2019). On the other hand, developmental temperature can change outcomes, for example, sex determination in reptiles (Ferguson and Joanen, 1982; Gutzke and Crews, 1988). Already before 1920, studies in *Drosophila* revealed temperature dependencies of the development of fly legs (Hoge, 1915), wings (Roberts, 1918), and eye facet numbers (Seyster, 1919). More than 100 years later, the *Drosophila* connectome is being finalized on the basis of specimens that developed at 25°C (Bates et al., 2020; Li et al., 2020; Scheffer et al., 2020; Takemura et al., 2015). Information about how the connectome might differ after development at a different temperature is currently not available.

In this study, we quantitatively investigated the influence of developmental temperature on brain development from subcellular neuronal filopodial dynamics to synapse numbers, synaptic partnerships, neuronal branch complexity, and behavior. We show that all developmental parameters quantitatively depend on developmental temperature. Specifically, lower temperature leads to an increase in synapse numbers and partnerships based

on increased availability of axo-dendritic branches and filopodia. For R7 photoreceptor neurons, we show that this increased availability leads to synapses with the same non-canonical synaptic partners as ablation of R7's preferred postsynaptic partner. Synapse formation based on relative synaptic availability leads to stable ratios of majority synapses, while total synapse numbers scale inversely with developmental temperature. Multiparametric behavior measurements in a visual choice assay revealed that adult movement activity is highly dependent on, and optimized for, the temperature at which the flies developed. We propose that evolution has selected for a *Drosophila* genome that can develop functional, but non-identical, brains through scalable synapse formation based on relative availability of synaptic partners during development.

RESULTS

Drosophila pupal development, the time during which the adult brain is wired, is almost precisely twice as fast at 25°C compared with 18°C (2.04 times faster, 98 versus 201 h) (Kohrs et al., 2021). In theory, every molecular and cellular developmental process could be sped up by a factor of 2 at 25°C, which would result in identical outcomes after development at both temperatures (Figure 1A). Alternatively, development at 18°C and 25°C could in fact lead to different outcomes. To quantitatively test how developmental processes and outcomes scale with developmental temperature, we devised a set of assays ranging from subcellular dynamics to behavior (Figure 1A).

Subcellular dynamics and synapse formation of R7 photoreceptor neurons inversely scale with developmental temperature

R7 photoreceptors in the *Drosophila* visual system are a well-studied model for axon targeting and synapse formation in a columnar and layered brain region *in vivo* (Figure S1A) (Douthit et al., 2021; Hadjieconomou et al., 2011; Kolodkin and Hiesinger, 2017; Trush et al., 2019). To measure the temperature dependency of subcellular dynamics, we first performed live imaging of developing R7 axon terminals during synapse formation, for which we have previously described the underlying quantitative dynamics (Özel et al., 2015, 2019). First, we measured the temperature dependency of filopodial dynamics that are known to mediate synapse formation and partner choice (Figure 1B) (Kiral et al., 2020; Kolodkin and Hiesinger, 2017; Özel et al., 2019). At 18°C, filopodia were 1.39 times slower and exhibited 1.52 times longer lifetimes compared with 25°C (Figures 1C and 1D; Video S1; Table S1). These measurements reveal a temperature dependency compared with a theoretical complete robustness to temperature (factor of 1); however, these values are less than the increased speed of pupal development at 18°C or 25°C (factor of 2). Development at 29°C (at the upper end of tolerable fly developmental temperatures) further exacerbated this effect (Figures 1C and 1D; Video S1). The relative frequency of synaptogenic filopodia with longer lifetimes (marked by bulbous tips and increased stability) was increased in a similar range at lower temperatures (Figure 1E). Hence, subcellular dynamics that underlie the development of synaptic connectivity differ significantly at different developmental temperatures, but not as much as overall pupal developmental tempo.

The kinetics of synaptogenic (bulbous) filopodia throughout development allow to quantitatively predict adult synapse numbers, as previously shown in a computational model of this process (Kiral et al., 2020; Özel et al., 2019). On the basis of 60 min live imaging data, we calculated that at 18°C, synaptogenic filopodia had a probability of 69% to live for at least 60 min, which reduced to 45% at 25°C and 23% at 29°C; synaptogenic filopodia lifetimes were 1.52 times higher at 18°C compared with 25°C (Figure 1F; Table S1). On the basis of these lifetime measurements, a Markov state model simulation predicts the progression of synapse formation throughout pupal development; the model accurately recapitulates progression of synaptogenic filopodia occurrences (Figure 1G) and predicts significantly different synapse numbers after development at the three different temperatures (Figure 1H; see Mathematical modeling in STAR Methods). To test these predictions, we measured synapse numbers immediately after pupal development at 18°C, 25°C, and 29°C using three independent methods.

First, we used the presynaptic release site marker BrpD3 probe (Fouquet et al., 2009), which revealed significantly increased numbers following development at lower temperature (Figures 1I–1L). Adult synapse numbers after development at the three different temperatures were in line with the model predictions (Figure 1L; Table S1).

Second, to count synaptic connections on the basis of synaptically connected postsynaptic partners of R7 neurons, we used a specific driver line that labels a subset of R7 neurons named yellow R7 (yR7) (reviewed in Rister et al., 2013) and the genetically encoded transsynaptic tracer technique *trans*-Tango (Talay et al., 2017). Adult connectivity on the basis of *trans*-Tango revealed a 1.26-fold increase in postsynaptically connected partners after development at 18°C compared with 25°C (Figures 2A–2D; Table S1). Remarkably, the *trans*-Tango labeling reproducibly identified several cell types after development at 18°C that are very rarely, or not at all, postsynaptically connected to yR7 photoreceptors according to available connectome data (Takemura et al., 2015). In particular, we found R7 synaptic connections to interneurons of the C2/C3 cell type (zero synapses in the connectome), Tm9 cells (zero synapses in the connectome), and Mi cell types including Mi1 and Mi4 (zero to two synapses in the connectome) (Figure 2A; Figures S1A and S1B). Notably, the electron microscopy-based connectome data are based on a specimen that developed at 25°C. Correspondingly, and consistent with the connectome data, these synaptic connections were not detected in *trans*-Tango experiments after development at 25°C or 29°C (Figures 2B–2D). These findings suggest increased synapse numbers after developmental at lower temperatures that can include synaptic partners excluded at higher developmental temperatures.

To control for the reported temperature dependency of the *trans*-Tango method (Talay et al., 2017), the newly hatched flies of all experimental groups were kept at 25°C for 1 week and treated identically for the *trans*-Tango labeling protocol. In addition, we tested the temperature dependency of the method during the first week of adulthood during which most

CellPress
OPEN ACCESS

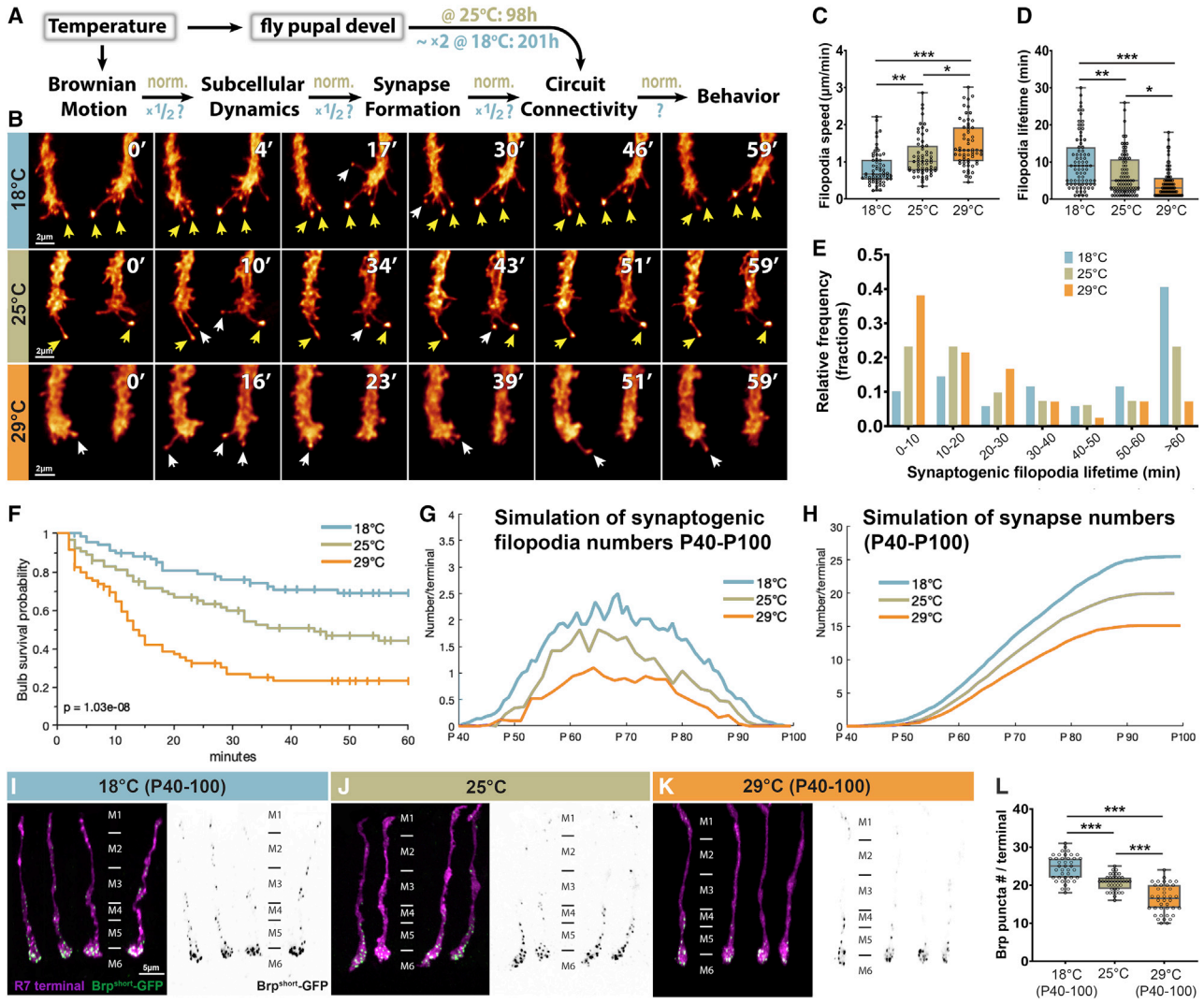

Figure 1. Temperature dependency of synapse formation in the R7 photoreceptor neuron

(A) Schematic of temperature effects during pupal developmental.

(B) Live imaging of filopodial dynamics during the time period of synapse formation (1 h with 1 min time lapse; yellow arrows, long-lived synaptogenic filopodia; white arrows, short-lived synaptogenic filopodia).

(C) Filopodial extension/retraction speeds are highly temperature dependent. n = 80 terminals (eight flies) per condition.

(D) Filopodial lifetimes are temperature dependent. n = 80 terminals (eight flies) per condition.

(E) The relative frequency of long-lived synaptogenic filopodia is temperature dependent. n = 23 terminals (eight flies) per condition.

(F–H) Computational modeling predicts how the measured filopodia dynamics affect synapse formation. (F) Calculation of synaptogenic filopodia survival probabilities on the basis of measured lifetimes. (G) Computational modeling of synapse development between P40 and P100 on the basis of synaptogenic filopodia dynamics. (H) Computational modeling of synapse number development between P40 and P100 on the basis of synaptogenic filopodia dynamics at different developmental temperatures.

(I–L) Synapse numbers on the basis of counts of the presynaptic active zone marker GFP-BrpD3 (Brp^{short}) are dependent on the developmental temperature between P40 and P100. n = 40 terminals (six flies) per condition.

Data were analyzed using the Kruskal-Wallis test and Dunn's post hoc test; *p < 0.0332, **p < 0.0021, and ***p < 0.0002.

the *trans*-Tango signal develops. In contrast to developmental temperature, 7 days at 18°C, 25°C, or 29°C during adulthood did not lead to differences in the number of labeled postsynaptic cells (Figure S2). Hence, both *trans*-Tango labeling and brpD3 labeling indicate a similar dependency of synapse numbers on developmental temperature. These synaptic connections remain stable for several days in the adult.

As a third method to validate changes of synapse numbers found in both BrpD3 active zone counts and *trans*-Tango experiments, we probed specific synaptic connections using the activity-dependent GRASP method (Macpherson et al., 2015). We first test synapse numbers between yR7 and its main postsynaptic partner neuron, the amacrine-like cell type Dm8 (Karuppudurai et al., 2014; Menon et al., 2019). Consistent with the connectome

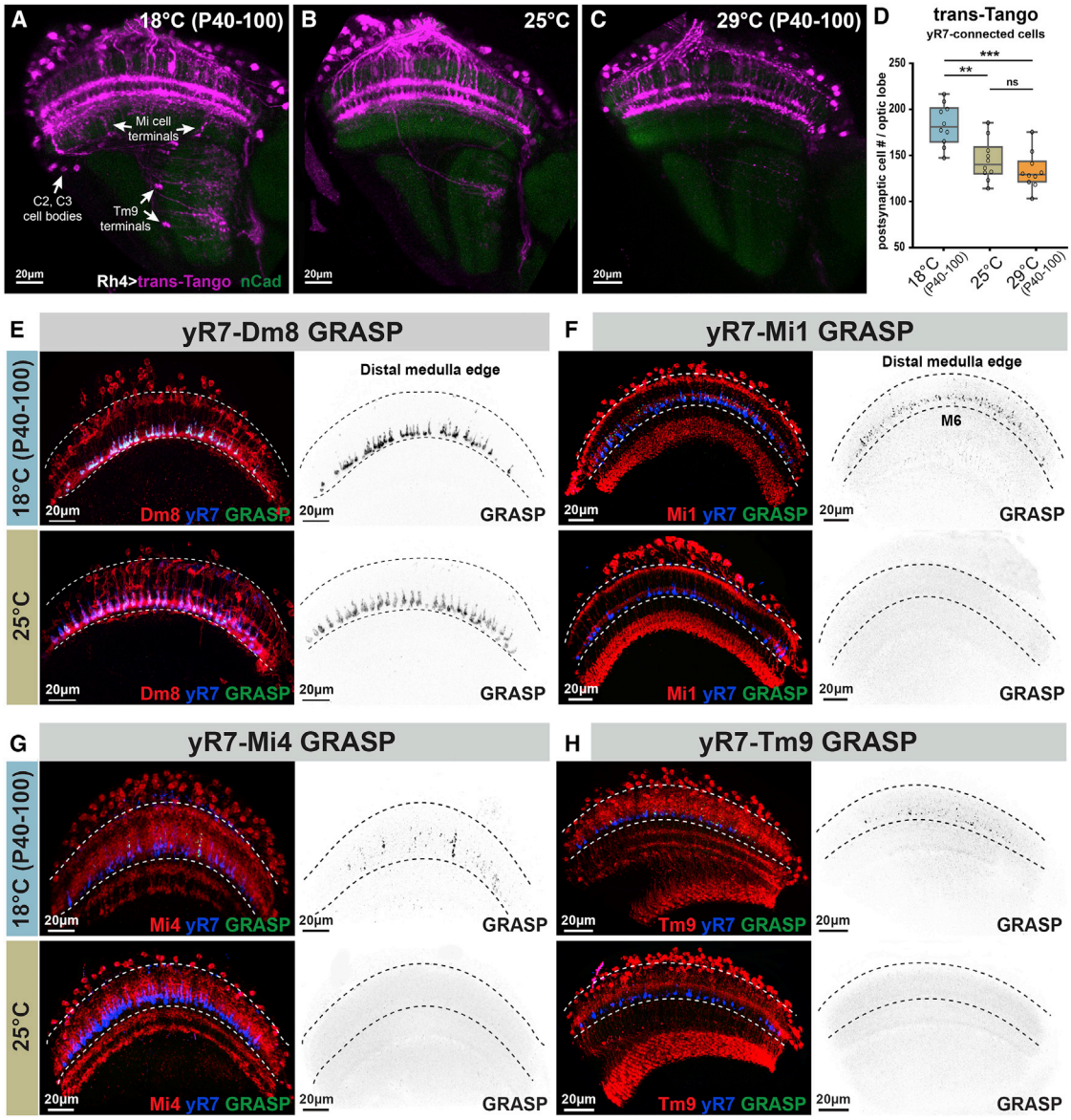

Figure 2. Synaptic connectivity scales with developmental temperature and includes additional, non-canonical synapses of yR7 photoreceptors at lower temperature

(A–C) Representative images of neurons (in magenta) that are postsynaptically connected to R7 neurons on the basis of the genetically encoded transsynaptic tracer method *trans*-Tango (Talay et al., 2017). See Figure S1A for identified cell types.

(D) Quantification of cell body counts of *trans*-Tango-labeled postsynaptic cells per optic lobe. n = 10 optic lobes (from ten flies) per condition.

(E–H) Validation of active synapses using the activity-dependent GRASP method (Macpherson et al., 2015) for the main postsynaptic partner Dm8 (E) and three identified postsynaptically connected neurons seen in (A) after development at 18°C that are not known to be synaptically connected on the basis of published connectome information. Blue, yR7; red, the potential postsynaptic partner; green, activity-dependent GRASP signal (reconstituted GFP). Black/white panels, single channel of the green GRASP signal.

Data were analyzed using the Kruskal-Wallis test and Dunn's post hoc test; *p < 0.0332, **p < 0.0021, and ***p < 0.0002; ns, not significant.

data, activity-dependent GRASP produced a strong signal precisely and selectively in the region where yR7 and Dm8 are known to forms synapses (Figures 2E and S3). The synaptic labeling was 1.24 times stronger after development at 18°C compared with development at 25°C (Figure S3C), in line with the increases in synapse numbers found using the presynaptic active zone marker (Figure 1L) and *trans*-Tango (Figure 2D). Finally, computational modeling based on measured filopodial dynamics yields the same numbers. We conclude that R7 synapse numbers inversely scale with developmental temperature on the basis of four independent measurement methods.

Next, we validate the synaptic partnerships seen in transsynaptic labeling after development at 18°C (but not at higher developmental temperatures) using activity-dependent GRASP.

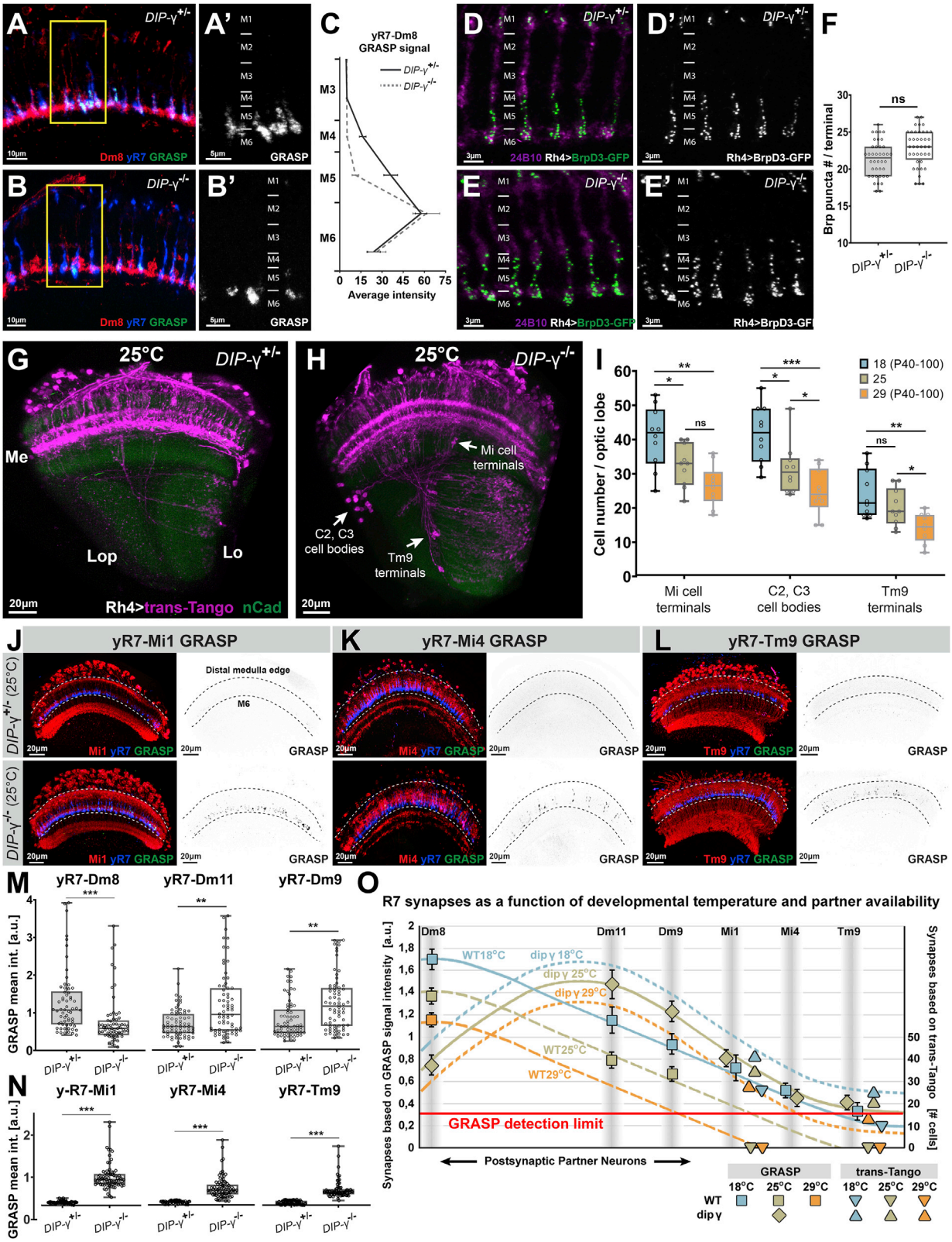

(legend on next page)

Specifically, we tested interneurons Mi1, Mi4, and Tm9, for which the connectome analyses of a specimen that developed at 25°C have so far identified very few or no synapses. These are, specifically, two R7-Mi1 synapses in 1 of 18 reconstructed Mi1s, one R7-Mi4 synapse in 1 out 16 reconstructed Mi4s, and zero R7-Tm9 synapses in 11 reconstructed Tm9s (Takemura et al., 2015). We therefore refer to these synapses as "non-canonical" synapses. Consistent with the connectome data, we found no GRASP signal between yR7 and Mi1, Mi4, or Tm9 after brain development at 25°C (Figures 2F–2H). In contrast, brain development at 18°C leads to robust labeling of these non-canonical synapses in exactly the layers in which their axonal and dendritic processes are present (Figures 2F–2H). We conclude that development at 18°C leads to a significant increase of R7 synapses that includes both the main synaptic partner Dm8 as well as synaptic partners excluded during faster brain development at higher temperature.

We have previously shown that loss of autophagy in R7 photoreceptors leads to increased stability of synaptogenic filopodia and increased synapse formation with Dm8 as well as non-canonical postsynaptic partner neurons (Kiral et al., 2020). The observation that lower temperature alone is sufficient to increase synapse formation with both canonical and non-canonical partner neurons suggests a model whereby all possible partner neurons increase their availability similarly (i.e., synaptic availability scales inversely with developmental temperature). For non-canonical partner neurons, this model predicts no or almost no synapses after development at higher temperature, while canonical synapses decrease equally with increasing temperature, thereby maintaining relative synaptic ratios (Figure 3O). Hence, synapse formation based on relative availability can in theory confer robustness to developmental temperature without keeping synapse numbers constant.

Loss of yR7's main postsynaptic partner neuron increases relative availability of the same non-canonical partners as development at lower temperature in wild-type

To test relative partner availability and its role in temperature-dependent scaling of synapse numbers, we devised an experiment to change the availabilities of canonical and non-canonical postsynaptic partner neurons of yR7 photoreceptors. The yR7 subtype constitutes 65% of the total R7 population and specifically expresses the cell surface molecule Dpr11, while the second R7 subtype is Dpr11 negative. Correspondingly, the matching postsynaptic Dm8 partner neuron expresses the interacting partner molecule DIPγ, while the non-matching Dm8 neurons are DIPγ negative. Loss of this molecular interaction leads to cell death of the majority of DIPγ(+)Dm8 neurons (Carrillo et al., 2015). Surprisingly, the synapse numbers in presynaptic yR7 terminals remain unaltered in a *dpr11* mutant despite the loss of DIPγ(+)Dm8 neurons (Xu et al., 2018). If yR7s maintain their synapse numbers in the absence of their major synaptic partner, what other synaptic partner neurons do yR7 terminals recruit, and does their recruitment scale with different developmental temperatures similar to wild-type?

To answer these questions, we first analyzed synapses between yR7 and possible partner neurons in a DIPγ mutant. We first validated the previously reported widespread loss of (about two-thirds of) Dm8 cells in this mutant (Figures S4A–S4C). Loss of DIPγ(+)Dm8 cells is specific to columns containing the yR7 subtype and easily recognized by the loss of a Dm8 distal protrusion, also called "sprigs," in such columns (Courgeon and Desplan, 2019; Menon et al., 2019); the sprigs mark an extended region of synaptic contacts between R7 and Dm8 cells (Figures S4D and S4E). Correspondingly, we find less activity-dependent GRASP signal between yR7 neurons and Dm8 cells in the region of the missing sprigs because of missing DIPγ(+) Dm8 cells (Figures 3A–3C). Note that we used a Dm8 cell driver that expresses in both Dm8 subtypes, and in the absence of two-thirds of all DIPγ(+)Dm8 cells, active synapses with DIPγ(−)Dm8 cells and remaining DIPγ(+)Dm8 cells are detectable. Indeed, the most proximal region of yR7 terminals exhibits levels of activity-dependent GRASP between yR7 and Dm8 that are indistinguishable from control even in the absence of the matched DIPγ(+) Dm8 in the home column (Figures 3B and 3C). Dm8 neurons are amacrine-like interneurons that extend axo-dendritic branches across more than ten columns; consequently, a yR7

Figure 3. Loss of the postsynaptic partner neuron DIPγ(+)Dm8 reveals synapse formation of yR7 neurons on the basis of relative availability

(A and B) Activity-dependent GRASP between yR7 and Dm8 neurons in a DIPγ mutant lacking DIPγ(+)Dm8 neurons and in a heterozygous control.

(A′ and B′) Single-channel GRASP signal.

(C) GRASP signal intensity along the yR7 terminals reveals a loss of signal in the absence of DIPγ(+)Dm8 "sprigs" between M4 and M5 but no reduced intensity in the main synaptic layer M6.

(D–F) Synapse numbers on the basis of counts of the presynaptic active zone marker GFP-BrpD3 are not significantly altered in the DIPγ mutant. n = 40 terminals (8 flies) per condition.

(G and H) Representative images of the postsynaptically connected neurons (magenta) to yR7 on the basis of the genetically encoded transsynaptic tracer method *trans*-Tango. Note that the same additional cell types are present in the DIPγ mutant (H) as in wild-type after development at 18°C (Figure 2A).

(I) The number of non-canonical postsynaptic partners in the DIPγ mutant is dependent on the developmental temperature; the mutant relative connectivity scales with temperature similar to wild-type. n = 10 optic lobes (from 10 flies) per condition.

(J–L) Validation of active synapses using the activity-dependent GRASP method (Macpherson et al., 2015) for three non-canonical postsynaptically connected neurons identified in (H) in a DIPγ mutant lacking DIPγ(+)Dm8 neurons and in a heterozygous control that developed at 25°C. Blue, yR7; red, the potential postsynaptic partner; green, activity-dependent GRASP signal (reconstituted GFP). Black/white panels, single channel of the green GRASP signal.

(M) Mean signal intensities of activity-dependent GRASP between yR7 and canonical partners (Dm8, Dm9, and Dm11) in a DIPγ mutant lacking DIPγ^+Dm8 neurons and in a heterozygous control. n = 70–80 terminals (10–12 flies) per condition.

(N) Mean signal intensities of activity-dependent GRASP between yR7 and non-canonical partners (Mi1, Mi4, Tm9) in a DIPγ mutant lacking DIPγ(+)Dm8 neurons and in a heterozygous control. n = 70–80 (9–12 flies) terminals per condition.

(O) A model based on GRASP and *trans*-Tango measurements that predicts no synapse formation between R7 and non-canonical partners (Mi1, Mi4, and Tm9) at higher developmental temperatures, while maintaining relative synaptic ratios of canonical partner neurons (Dm8, Dm9, and Dm11).

Data were analyzed using the Kruskal-Wallis test and Dunn's post hoc test; *p < 0.0332, **p < 0.0021, and ***p < 0.0002; ns, not significant.

axon terminus with a missing matched DIPγ(+)Dm8 neuron is not prevented from forming synapses with processes from neighboring Dm8s despite their lack of the DIPγ, suggesting that DIPγ is not required for synapse formation between yR7 and Dm8 cells.

Because of the reduced number of synapses in the sprig region, the activity-dependent GRASP analysis between yR7 and Dm8s suggests an overall reduction of synapses between these two cell types (Figure 3C). However, our synapse counts based on the presynaptic marker BrpD3 indicate that yR7 synapse numbers in the DIPγ mutant were not significantly altered (Figures 3D–3F), in agreement with previous synapse counts in the *dpr11* mutant yR7s (Xu et al., 2018). To identify other postsynaptic partners, we performed *trans*-Tango experiments in the DIPγ mutant (at 25°C developmental temperature and using a +/DIPγ heterozygote as control; Figures 3G and 3H). Remarkably, *trans*-Tango labeling in the DIPγ mutant optic lobe after development at 25°C looked very similar to a wild-type optic lobe after development at 18°C, prominently including postsynaptically connected C2/3 cells, Tm9 cells, and Mi cells (compare Figures 3H and 2A). A cell-by-cell comparison revealed identical postsynaptically connected neurons for 18°C wild-type and 25°C DIPγ mutant brains (Figures S1A–S1C).

Our transsynaptic tracing results suggest that loss of DIPγ increases the relative availability of non-canonical partner neurons in a manner similar to lower developmental temperature in wild-type (i.e., by increasing the pool of possible postsynaptic partners). Although in wild-type the non-canonical synapses are effectively absent after development at 25°C or above, their overall increase in the DIPγ mutant makes it possible to test for their relative frequency at different temperatures. We found that the number of transsynaptically labeled low-probability Mi1/4-yR7, C2/3-yR7, and Tm9-yR7 synaptic connections could be dialed down at 29°C and dialed up at 18°C, while maintaining their relative frequencies (Figure 3I; Figures S4F and S4G). These findings indicate robustness of relative frequency to different developmental temperatures without keeping total synapse numbers constant, similar to our observation for canonical synapses in wild-type (Figure 3O).

To validate the *trans*-Tango results, we performed activity-dependent GRASP experiments for the non-canonical pairings yR7-Mi1, yR7-Mi4, and yR7-Tm9 in control and DIPγ mutants after development at 25°C. As in wild-type (Figures 2F–2H) and in the available connectome data, the +/DIPγ heterozygote control exhibited no or very rare GRASP signals for these non-canonical synapses. In contrast, the non-canonical synapses were prominent in the DIPγ mutant in the correct layer of their known axo-dendritic overlap and looked virtually indistinguishable from the wild-type GRASP signal after development at 18°C (Figures 3J–3L; compare Figures 2F–2H). Similarly, activity-dependent GRASP analyses of cell types that are known to be synaptically connected to yR7 (Dm9 and Dm11 cells) revealed similar increases of synaptic labeling in the DIPγ mutant (Figures S5A–S5G; Table S2). These findings indicate that a loss or reduction of the number of DIPγ(+) Dm8 cells creates a situation in which yR7 neurons recruit more synaptic partners from a pool of both canonical (Figure 3M) and non-canonical (Figure 3N) partners. The recruitment of these alternative synaptic partners appears to be specific to those that have dendritic arborizations in the correct medulla layer, as Dm3 and Dm6 cells never form synapses with yR7 in control of the DIPγ mutant (Figures S5H–S5K). Despite these shifts in synaptic partnerships, the final number of yR7 synapses is not significantly different from wild-type at the same developmental temperature (Figures 3F and 1L). These findings suggest a presynaptic mechanism for the determination of synapse numbers independent of the types of postsynaptic partners, consistent with the presynaptic serial synapse formation model for R7 (Özel et al., 2019) as well as previous observations for R1–R6 photoreceptors (Hiesinger et al., 2006). We conclude that the absence of Dm8 neurons increases the relative availability of other possible R7 partner neurons, in effect "filling vacant Dm8 slots" up to the number observed in wild-type for a given temperature.

In sum, our analyses of yR7 synapse formation as a function of developmental temperature and partner availability revealed that overall synapse numbers increase with lower temperatures, including low-probability synapses not observed at higher temperatures. By contrast, relative synaptic frequencies are robust to different developmental temperatures unless a type of synapses drop to zero at a higher temperature (Figure 3O).

Morphogenesis and synapse formation of branched interneurons in the brain depend on developmental temperature

To what extent is the temperature dependency of neuronal development and synapse formation a general phenomenon in the fly brain? To approach this question, we analyzed a series of neuron types that face diverse challenges during the establishments of synaptic partner contacts.

First, we analyzed photoreceptors R1–R6, which terminate in a different brain region from R7, the lamina; in contrast to R7, growth cones of R1–R6 need to undergo a lateral sorting process to form a functional visual map required for motion vision according to the principle of neural superposition (Agi et al., 2014; Hadjieconomou et al., 2011; Langen et al., 2015), and their functional output can be estimated on the basis of electroretinogram (ERG) recordings (Pak et al., 1969). Similar to our findings for R7, synapse numbers of adult R1–R6 increased by a factor of 1.15 on the basis of the presynaptic BrpD3 marker after development at 18°C compared with development at 25°C (Figure 4A; Figures S6A–S6D). Synaptic transmission (as measured by the ERG "on" transients) was significantly increased after development at 18°C compared with 25°C, consistent with increased numbers of synaptic connections (Figures 4B and 4C; Figures S6E and S6F). These findings indicate that the increased numbers of synapses after development at 18°C compared with 25°C are functional. In contrast, phototransduction (i.e., the ability of R1–R6 to convert a light stimulus into an electrical signal in the cell body, as measured by the ERG depolarization component) revealed no significant differences after development at different temperatures (Figures S6E and S6G). We conclude that although phototransduction is unaffected by variability of developmental temperatures, synapse numbers and neurotransmission are increased after development at a lower temperature.

Next, we analyzed Dm8 neurons, the main synaptic partner neuron of R7 photoreceptors, whose dynamic and competitively regulated branch development has recently been analyzed in

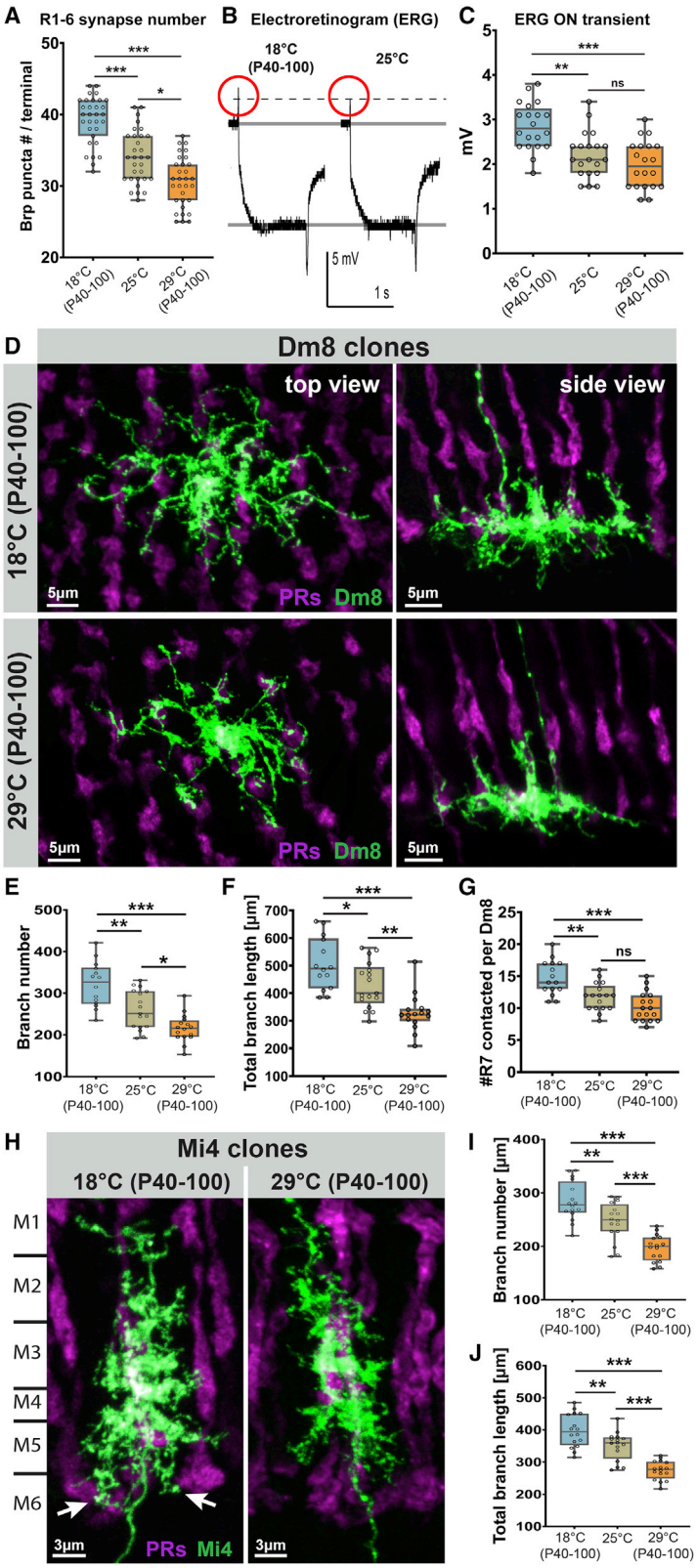

Figure 4. Neurotransmission of R1–R6 photoreceptors and branch morphology of Dm8 and Mi4 interneurons scale with developmental temperature

(A) R1–R6 photoreceptor synapse numbers on the basis of counts of the presynaptic active zone marker GFP-BrpD3 (Brp^{short}) depend on the developmental. n = 30 terminals (6 flies) per condition.

(B) Representative electroretinogram (ERG) traces recorded from wild-type (WT) fly eyes developed at different temperatures.

(C) Development at lower temperature increases neurotransmission of R1–R6 photoreceptors on the basis of ERG "on-transient" amplitudes. n = 20 flies per condition.

(D) Single-cell clone representative images of Dm8 neurons developed at low (18°C, P40–P100) and high (29°C, P40–P100) temperatures.

(E–G) Dm8 neurons exhibit increased branch numbers (E), total branch length (F), and numbers of R7 contact sites (G) after development at 18°C. n = 14–17 cells (6 flies) per condition.

(H) Single-cell clone representative images of Mi4 neurons developed at low (18°C, P40–P100) and high (29°C, P40–P100) temperatures. White arrows point to Mi4 branches invading M6 medulla layer after development at 18°C where R7s are synaptically most active.

(I and J) Mi4 interneurons (which are only connected to yR7 neurons after development at 18°C or in the absence of Dm8s) also exhibit increased branch numbers (I) and total branch lengths (J) after development at 18°C. n = 16 terminals (7 flies) per condition.

Data were analyzed using the Kruskal-Wallis test and Dunn's post hoc test; *p < 0.0332, **p < 0.0021, and ***p < 0.0002; ns, not significant.

detail (Luo et al., 2020). The overall morphology of Dm8 neurons (Figure 4D), including branch numbers (Figure 4E) and total branch lengths (Figure 4F) differed markedly depending on the developmental temperature. As Dm8 extends its branches across several medulla columns, the temperature dependency of its branch morphology leads to on average of 14 columns contacted by a single Dm8 after development at 18°C, 12 columns after development at 25°C, and 10 columns after development at 29°C (Figure 4G; Figures S6H–S6J). These findings correspond well with the temperature dependency of synapse numbers between yR7 and Dm8 (Figures 2E and S3C; Table S1). The observations further suggest that increased branching of the canonical R7 partner Dm8 increases its availability for synapse formation.

To test whether increased availability through increased branching also occurs for a non-canonical partner of R7 photoreceptors, we analyzed Mi4 neurons after development at different temperatures. Similar to Dm8 neurons, Mi4 neurons exhibited a comparable temperature dependency of both branch numbers and total branch lengths (Figures 4H–4J; Table S1). Taken together, these findings suggest that visual interneuron branching, photoreceptor filopodial dynamics, and synapse formation all scale with similar ratios with developmental temperature (Table S1).

Next, we analyzed the effect of developmental temperature on two other neuron types outside the *Drosophila* visual system. First, we searched the Fly Light split-Gal4 collection for sparsely labeled central nervous system neurons and chose descending neurons as candidates (Namiki et al., 2018). We selected DNp24 neurons (line SS00732) for quantification because of its distinct axonal arborizations and the strength of the Gal4 driver line (Figure S7A). The number of DNp24 branch terminals was significantly reduced after development at higher temperature (Figure S7B), while the overall area covered by branches was not significantly different (Figures S7C–S7F). These findings show that axonal branches can cover similar regions with variable numbers of branches.

Finally, we analyzed the effect of temperature on dendritic development of adult motoneurons. We selected motoneurons MN1–5 that innervate the dorsal longitudinal flight muscle (DLM). MN1–5 have dendrites of similar sizes that intermingle in the same space of the flight neuropil. We have previously characterized the dendritic architecture of MN5 in animals raised at 25°C throughout development (Vonhoff and Duch, 2010), as well as MN5's activity-dependent development on the basis of intra-neuronal competition (Ryglewski et al., 2017). Using the same intracellular filling technique as in the previous studies, we therefore analyzed MN5 dendritic branching structure after development at all three temperatures on the basis of geometric three-dimensional (3D) reconstructions (Evers et al., 2005), one for each temperature (Figures S8Ai–S8Ci). Developmental temperature only had no or very mild effects on the total number or the mean radius of dendritic branches (MDR; Figure S8D) or the mean length of dendritic branches (MDL) and total dendritic length (TDL) (Figure S8D). In contrast, the organization of dendritic branches within the tree was remarkably different: dendritic trees after development at 18°C contained increased branch numbers at higher orders (i.e., branches that formed on other branches: up to 50 or 60 levels), whereas dendritic trees that developed at higher temperature contained increased branch numbers at lower orders and decreased branch numbers at high orders (Figure S8E). Given that low branch orders form earlier than high order branches, this indicates that increased temperature causes increased early branch formation but decreased late branch formation. We conclude that developmental temperature can have different effects on different neuron types that require type-specific investigation.

Dorsal cluster interneurons scale filopodial dynamics, branching, synapse numbers, and synaptic partnerships with developmental temperature

To analyze temperature-dependent developmental dynamics, branching, and synapse formation in a large interneuron that has been shown to directly affect behavior, we focused on contralaterally projecting interneurons called dorsal cluster neurons (DCNs). DCNs form highly distinctive branched axonal patterns in the contralateral brain hemisphere (Figure 5A); differences in these patterns predictively and quantitatively affect individual fly behavior (Linneweber et al., 2020). Similar to Dm8 and Mi4, we found that DCNs exhibited increased numbers of branches after development at 18°C compared with 25°C and 29°C (Figures 5B–5D). To observe the development of the different branching patterns, we established multiphoton live imaging of branching dynamics in the intact developing brain on the basis of our *ex vivo* imaging culture system (Özel et al., 2015). Time-lapse videos obtained during development at all three temperatures revealed a significant temperature dependency of extension and retraction speeds, similar to R7 axon terminals (Figures 5E–5G; Video S2; compare Figures 1B–1D and Video S1). Correspondingly, synapse numbers based on the BrpD3 presynaptic marker were increased after development at 18°C compared with 25°C and 29°C (Figures 5H–5J).

To validate the temperature-dependent scaling of synapse numbers and connectivity, we performed both *trans*-Tango and GRASP labeling of synaptic connections, similar to our analyses of R7 neurons. Transsynaptic tracing of postsynaptically connected cells with *trans*-Tango revealed a significant difference in the number of labeled postsynaptic cells after development at 18°C compared with 25°C, similar to our findings for R7 neurons (Figures 5K–5M). We identified several of the postsynaptically connected neurons on the basis of morphology, including Lamina widefield (Lawf) interneurons as well as at least two more rarely connected cell types (L cells and Lpi cells) that we observed only after development at 18°C, but not 25°C (Figures S7D and S7E). To validate the temperature dependency of active synapses for these interneurons, we performed activity-dependent GRASP experiments between DCNs and Lawf1 neurons. We observed activity-dependent GRASP labeling of DCN-Lawf1 synapses after development at 18°C and to a significantly lesser degree after development at 25°C and 29°C; in all cases, the GRASP signal was specific to the brain region where DCN-Lawf1 contacts are predicted (Figures 5N–5P). As with R7 photoreceptors, the temperature-dependent scaling of connectivity is supported by independent measurements of life dynamics and synapse numbers on the basis of three independent methods. We conclude that slower development at

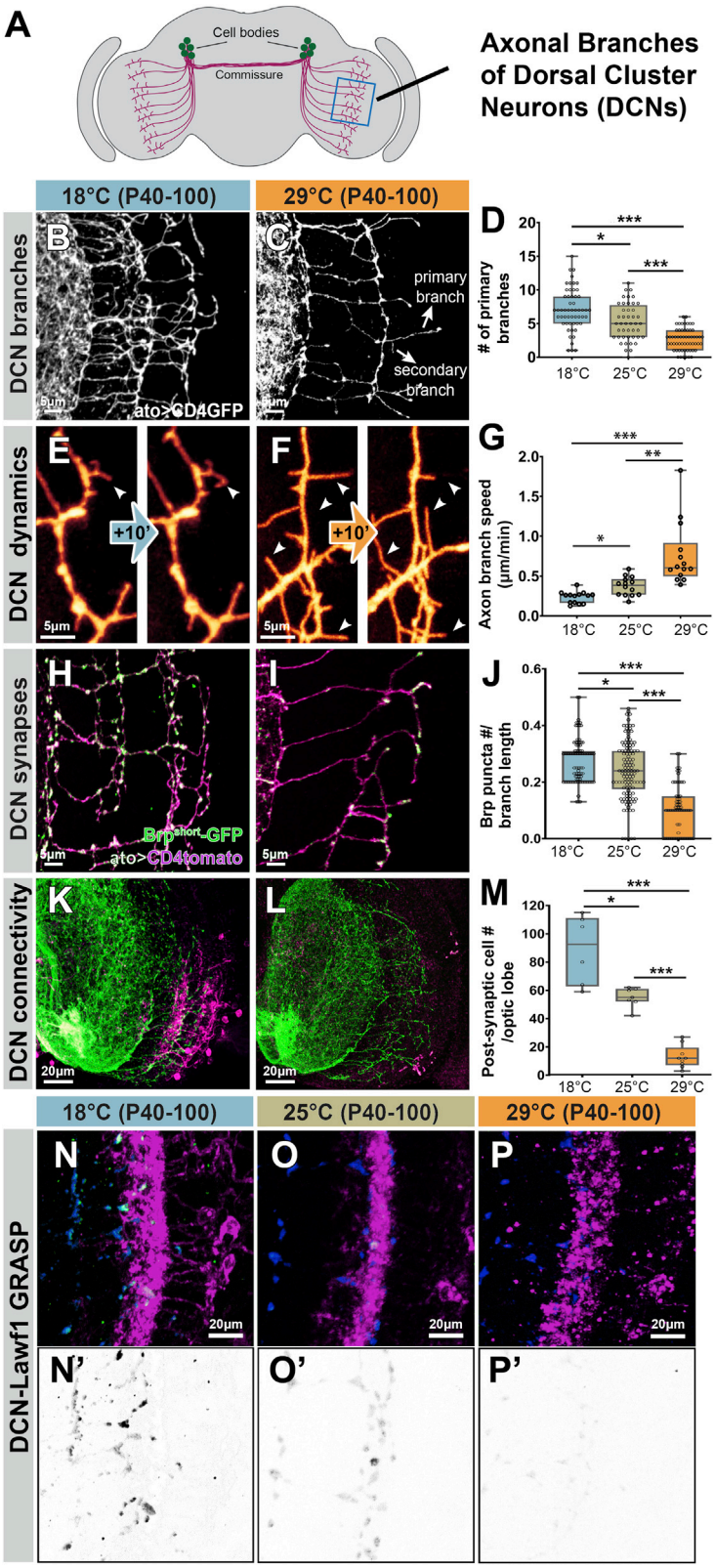

Figure 5. Branching dynamics, branch elaboration, synapse formation, and partnerships of dorsal cluster neurons scale with developmental temperature

(A) Schematic of dorsal cluster neurons (DCN) in the fly brain.

(B–D) DCNs exhibit increased number of axonal branches after development at 18°C. n = 45–58 branches (five to seven flies) per condition.

(E–G) Axonal branch dynamics of DCNs are highly temperature dependent. n = 14 branches (four flies) per condition.

(H–J) Synapse numbers based on the presynaptic active zone marker GFP-BrpD3 reveals increased synapse formation of DCNs after development at 18°C. n = 90–120 branches (six flies) per condition.

(K–M) DCNs form more postsynaptic connections after development at 18°C on the basis of transsynaptic tracing method *trans*-Tango. n = 6–9 optic lobes (from six to nine individual flies) per condition.

(N–P') Activity-dependent GRASP between DCN and Lawf2. Note increased GRASP signal after development at 18°C.

Data were analyzed using the Kruskal-Wallis test and Dunn's post hoc test; *p < 0.0332, **p < 0.0021, and ***p < 0.0002.

lower temperature leads to decreased dynamics and increased branching and synapse formation with a larger pool of postsynaptic partners in DCNs, similar to our findings for R7 photoreceptors.

Movement activity is adapted to the temperature at which the fly developed, while movement precision is largely unaffected by developmental temperature

The developmental temperature-dependent differences of DCN branch morphologies are quantitatively similar to differences in DCNs that are known to significantly affect behavior in a visual choice assay (Linneweber et al., 2020). This assay, Buridan's paradigm, is a multiparametric single-fly behavioral paradigm that allows to quantitatively measure more than 25 different parameters related to fly movements in response to defined visual stimuli (black bars on two sides of an arena; Figure 6Y) (Colomb et al., 2012; Linneweber et al., 2020). The assay is sufficiently sensitive to measure specific behavioral differences as a consequence of different DCN morphologies (Linneweber et al., 2020). We assessed 25 behavioral parameters that include measures related to overall activity (e.g., walking speed, pause lengths, overall walking distance), measures for movement angles or location that are independent of visual cues (e.g., the amount of turns taken or the time spent at or away from the center of the arena), and measures directly related to movement angles or location relative to the visual cues (Table S3). We tested a Janelia wild-type strain used for recent connectome analyses (Takemura et al., 2015) following development between P40 and P100 at different temperatures.

First, we tested flies after development at 18°C, 25°C, or 29°C at a "behavioral temperature" of 25°C. Most parameters related to overall activity were significantly lower after development at 18°C compared with 25°C (Figure S10), including number of walks (1.59 times more; Figure 6G), the total distance traveled (1.51 times more; Figure 6H), and pause durations (1.54 times less; Figure 6I). In contrast, parameters associated with movement angles or location relative to the visual cues were not significantly altered, such as axis deviation (Figure 6J), angle deviation (Figure 6K), and horizon deviation (Figure 6L). Hence, parameters related to the precision of movement angles were largely unaffected by different developmental temperatures, while general activity levels scaled with developmental temperature in a range similar to neuronal branch morphologies and synapse numbers (Tables S1 and S3).

The observed increased adult activity levels after development at 25°C and 29°C might be the result of a brain wired for more behavioral activity at any behavioral temperature, or a brain adapted for that exact behavioral temperature. The latter idea of adaptation would predict that development at 18°C might lead to more activity at 18°C. To distinguish between these possibilities, we performed experiments at the behavioral temperatures 18°C and 29°C. Measures for overall activity at behavioral temperatures 18°C and 29°C changed largely in agreement with the adaptation hypothesis. For example, flies that had developed at 18°C exhibited more overall activity at the behavioral temperature 18°C than flies that had developed at 25°C or 29°C (Figures 6A–6C and 6S–6U). On the other hand, flies that had developed at higher temperatures exhibited selectively increased overall activity at 25°C and 29°C (Figures 6S–6U). By contrast, similar to behavior at 25°C, most parameters associated with movement precision were not or only mildly affected (Figures 6D–6F, 6P–6R, and 6V–6X; Figures S11 and S12). We conclude that overall activity levels depend on developmental temperature in a manner that increases activity for the temperature at which the flies developed. These observations are consistent with evolutionary selection for functional flies, but not identical brains.

DISCUSSION

The genome contains information to grow network connectivity, not information that describes network connectivity. Selection occurs at the level of behavior, on the basis of developmental processes that are flexible enough to ensure robustness to variable environmental conditions (Hiesinger and Hassan, 2018). Many animals, including *Drosophila*, have evolved robustness of brain development to varying developmental temperatures. However, robustness does not need to ensure identical development or outcomes as long as the resulting connectivity is functional. In this study, we have shown that non-identical functional connectivity and adult behavior result from development at different temperatures. We propose that the underlying developmental processes do not specify synaptic connectivity in absolute terms but on the basis of scalable, relative availabilities of synaptic partners.

Temperature robustness through developmental synaptic scaling

We found temperature dependencies at every level from subcellular dynamics to synapse formation and circuit connectivity. However, the doubling of the developmental tempo at 25°C compared with 18°C is not accompanied by a doubling of the rate of synapse formation—or any other developmental parameter measured in our study. Instead, processes ranging from filopodial dynamics to branching and active zone formation were all only increased between ~1.2- and 1.8-fold (Table S1). Consequently, development in half the time with less than a doubling of synapse formation leads to fewer overall synapses at 25°C compared with 18°C. Synaptic ratios are robust to temperature if synapse numbers and types exhibit the same relative changes.

In brain function, synaptic scaling is well characterized as a means of homeostatic regulation of destabilizing variability (Turrigiano, 2012), with important consequences for learning and mental health (Kavalali and Monteggia, 2020; Turrigiano, 2017). Like its functional counterpart, developmental synaptic scaling may provide a basis for the maintenance of relative input strengths in neural circuits. Other mechanisms that have been shown to contribute to temperature robustness include ion channel degeneracy and regulation (Goaillard and Marder, 2021; O'Leary and Marder, 2016). However, we do not yet know how ion channel expression and regulation is affected by development at different temperatures. We speculate that developmental temperature may have differential effects on specific proteins such as ion channels, cytoskeletal proteins, and molecules of the transmitter release machinery, all of which contribute to circuit properties and ultimately behavior.

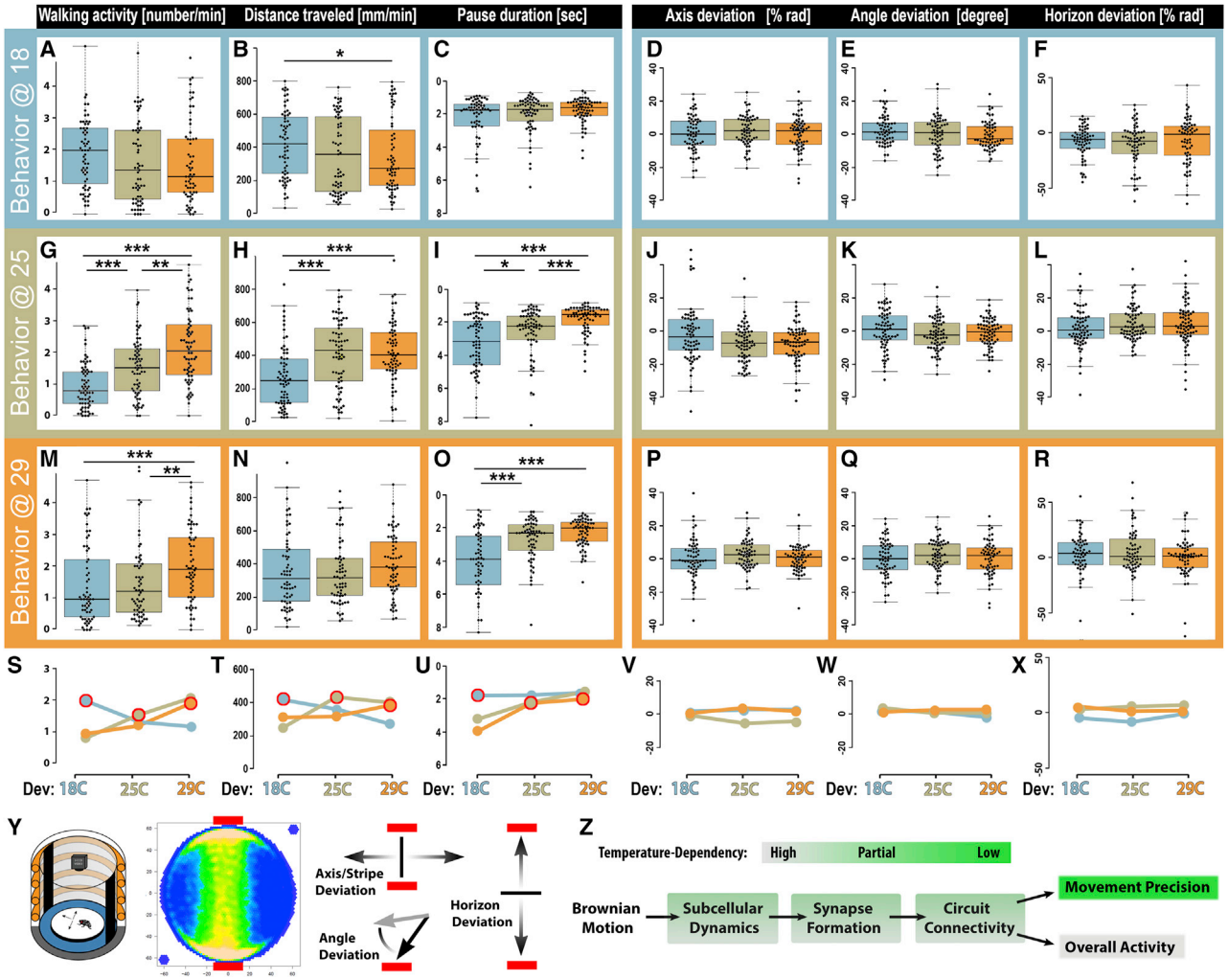

Figure 6. Developmental temperature affects overall movement activity but not movement precision

(A–R) Six of a total of 25 behavioral parameters analyzed for differences between adult behavior after development at 18°C, 25°C, or 29°C (colored boxplots) and the same three behavioral temperatures (colored borders). n = 70 flies per condition. Quantitative data in Table S3. Nine plots on the left: the three most significantly temperature-dependent behavioral parameters: walking activity (A, G, and M), distance traveled (B, H, and N), and pause duration (C, I, O). Nine plots on the right: three parameters that are largely unaffected by developmental temperature: axis deviation (D, J, and P), angle deviation (E, K, and Q), and horizon deviation (F, L, and R).

(S–X) Schematic plots based on the data in (A)–(R) showing the mean values for a behavioral temperature (indicated by graph color) in dependence of developmental temperature.

(Y) Buridan's paradigm (from left to right): experimental setup, heatmap of typical fly movement activity, illustrations of the parameters axis deviation, angle deviation, and horizon deviation.

(Z) Summary of temperature dependencies.

See Figures S10–S12 for all behaviors and STAR Methods for details on each parameter. Data were analyzed using the Kruskal-Wallis test and Dunn's post hoc test; *p < 0.05, **p < 0.01, and ***p < 0.001.

Similar to a lower temperature, reduced metabolism decreases the pace of *Drosophila* development and has recently been shown to increase robustness by decreasing developmental errors (Cassidy et al., 2019). Although the mechanism of error suppression in this study is likely different from the temperature effects observed here, we note that scalable relative connectivity is also likely more robust at lower temperatures because the synaptic ratio of high-probability synapses is established by larger numbers.

A contribution of relative synaptic partner availability to synaptic connectivity

The genome encodes developmental programs that produce remarkably precise synaptic connectivity. Yet individual neurons across animal species, taken out of the context of these developmental programs, readily form "incorrect" synapses, including with themselves (Bekkers and Stevens, 1991; Clements et al., 2008; Harris et al., 2020; Hiesinger et al., 2006; Van der Loos and Glaser, 1972). Even during normal development some

degree of synaptic promiscuity is prevalent, for example, as a basis for subsequent pruning or fine-tuning (Agi et al., 2020; Hassan and Hiesinger, 2015; Lieberman et al., 2019; Shatz, 1996; Wilton et al., 2019). The notion of promiscuous synapse formation on the basis of relative partner availability is not at odds with precise outcomes. Instead, it offers the opportunity to explain precision in the context of developmental plasticity and robustness to perturbation. The limiting case of "total promiscuity" (i.e., the ability of any neuron to form synapses with any other neuron) is highly unlikely given known molecular interactions that specify or bias connections (de Wit and Ghosh, 2016; Dudanova and Klein, 2013; Sanes and Zipursky, 2020; Südhof, 2018). At the other end of the spectrum, precise molecular key-and-lock mechanisms for all synapses represent the antithesis to promiscuous synapse formation: if the key does not fit the lock, a synapse should not form. This is equally unlikely, given the known ability, and often developmental necessity, to form synapses with variable partners.

Synapse formation requires proximity- and kinetics-based mechanisms involving locally restricted molecular machinery (Agi et al., 2020; Hoersting and Schmucker, 2021). In addition, molecular specificity or selectivity with a "hierarchy of preference" (Sanes and Zipursky, 2020) are principally consistent with developmental synaptic scaling, as more stable filopodia and branches will also increase, and thus scale, molecular recognition. However, such a molecular "hierarchy of preference" would have to include at least all the non-canonical synapses shown in this study for yR7 neurons and DCNs. To what extent molecular interactions play earlier developmental roles prior to synapse formation (Petrovic and Schmucker, 2015) and to what extent synapse formation could be promiscuous on the basis of specification through proximity and kinetics (Agi et al., 2020) remain a matter of debate (Hassan and Hiesinger, 2015; Hiesinger, 2021; Sanes and Zipursky, 2020).

Lower developmental temperature in wild-type flies increased numbers of synapses with both canonical and non-canonical partners, similar to previous observations in autophagy mutants (Kiral et al., 2020). Our findings suggest that temperature alone is sufficient to raise the availability of some synaptic partners above zero. Our distinction of canonical and non-canonical synapses is based solely on the probability to form synapses and their absence in EM connectome analyses on the basis of specimens that developed at 25°C (Scheffer et al., 2020; Takemura et al., 2015). The observation that the number of these non-canonical synapses is significantly increased after development at a lower but still physiological temperature opens the possibility that these synapses are functional and evolutionarily selected (or at least not selected against) parts of the connectome.

Genetically encoded brain wiring based on relative synaptic partner availability allows surprising variability among brains, even if genetically identical. Both stochastically encoded developmental processes (Linneweber et al., 2020) as well as environmental differences (this study) may contribute to such variability of genetically encoded brain wiring. Further support for this idea comes from recent comparative connectomics analyses in *C. elegans* demonstrating that more than 40% of all cell-cell connections are not conserved between isogenic worms (Witvliet et al., 2021).

Dpr11 and DIPγ function prior to, but not during, synapse formation

Our findings are consistent with the reported role of the Dpr11/DIPγ interaction for partner cell survival during a developmental process prior to synapse formation (Carrillo et al., 2015; Courgeon and Desplan, 2019; Menon et al., 2019). Loss of DIPγ leads to loss of the majority of DIPγ(+)Dm8 cells and, as we show here, a widening of the pool of possible partners for Dpr11-positive yR7 terminals during the later process of synapse formation. We conclude that in wild-type, the Drp11/DIPγ interaction-mediated survival of DIPγ(+)Dm8 cells effectively reduces the pool of postsynaptic partners by placing the main postsynaptic partner in close proximity and thereby increasing its relative availability.

Contrary to previous interpretations, we show that the actual synapse formation process does not use Dpr11/DIPγ interaction. Instead, yR7 axon terminals form a remarkably invariant number of synapses at a given temperature independent of the presence or absence of Dpr11 (Xu et al., 2018), DIPγ, or the main postsynaptic partner neuron Dm8 (this study). In a DIPγ mutant, yR7 axon terminals form synapses with non-matched Dm8s, plus other known synaptic partners based on the 25°C connectome, as well as available partners that are not, or very rarely, present in the 25°C connectome (Takemura et al., 2015). Remarkably, the additionally recruited synaptic partners are identical in a DIPγ mutant after development at 25°C and wild-type after development at 18°C. Hence, at least the cell types that are shown here to be recruited as postsynaptic partners during development at 18°C or in the absence of DIPγ(+) Dm8 cells are not prevented from synapse formation by molecular mismatch.

As both the number and the specificity of partnerships of yR7 synapses in the DIPγ mutant scale with developmental temperatures similar to wild-type, we propose that synaptic specificity is a developmental outcome of a composite of relative contributors that include spatiotemporal availability, interaction kinetics, and interaction biases through molecular recognition between partner cells (Hiesinger, 2021). In this view, the removal or alteration of a single relative contributor (e.g., the spatiotemporal availability of the main postsynaptic partner cell) increases the relative contribution of other factors, including the availability of other cells and their likelihood to form synapses on the basis of interaction kinetics (Agi et al., 2020; Kiral et al., 2020).

Increased *trans*-Tango labeling after development at 18°C reflects an actual increase in synapse numbers

The transsynaptic labeling technique *trans*-Tango has been known since its inception to label significantly more postsynaptic target cells at 18°C compared with 25°C. This effect could be the result of a technique-specific artifact or reflect a real temperature effect on the brain (Talay et al., 2017). Our data provide evidence for the latter hypothesis. As shown in Figure S2, the development of *trans*-Tango labeling over 7 days in the adult is identical at all temperatures. Hence, *trans*-Tango labels more cells only if the 2 critical days of late pupal development occur at lower temperature, not if 7 further days during adulthood occur at a lower temperature. Furthermore, we found the increased number of *trans*-Tango-labeled cells to be quantitatively validated with GRASP, brpD3-labeled active zones as well as

transgenics-independent measures including branch extensions and, in the case of R1–R6, neurotransmission on the basis of ERG recordings (see Table S1 for all parameters).

Developmental temperature adapts movement behavior for the same adult environmental temperature

Our description of behavioral differences in response to environmental changes during development is reminiscent of the often excruciatingly stringent developmental conditions required for fly behavioral assays. Our findings suggest that behavioral differences are a direct consequence of connectivity differences associated with different developmental temperatures. A direct relation of neuronal morphology and individual behavior was previously shown for DCN neurons (Linneweber et al., 2020). This study identified a relation of left/right DCN wiring asymmetry to the behavioral parameter "absolute stripe deviation," which is more related to movement precision. Indeed, we found no significant differences for this parameter after development at 18°C or 25°C at the behavioral temperatures 18°C and 25°C. Yet "absolute stripe deviation" did show some temperature dependency after development at 29°C and at the behavioral temperature of 29°C, suggesting increased asymmetry after development at 29°C or an exacerbation of behavioral differences at 29°C.

Our findings show that adult wild-type flies that developed at a lower temperature have more elaborately branched interneurons, have more synapses with more varied synaptic partners, and exhibit most overall movement activity at the same low temperature at which they developed, but mostly lower levels of overall activity at higher behavioral temperatures. In contrast, adult flies that developed at a higher temperature during time period of synapse formation have fewer branched interneurons, have fewer synapses with fewer synaptic partners, and exhibit more overall movement activity at higher behavioral temperatures than at lower temperatures. These findings are consistent with a preference of adult flies (Rajpurohit and Schmidt, 2016) and worms (Hedgecock and Russell, 1975) for the temperature at which they developed, but how the underlying connectivity difference cause behavioral adaptation remains to be determined. In *Drosophila melanogaster*, as in other species, evolution likely has selected a genome that encodes different brain connectivity at different developmental temperature to increase behavioral fitness.

Limitations of the study

Key to our study is the validation of non-canonical synapses using multiple methods, including synaptic markers, transsynaptic tracing, and activity-dependent split-GFP (GRASP). Yet electrophysiological recordings of synaptically connected neuronal pairs remain the gold standard to validated synaptic connectivity. Here, we only provided extracellular recordings of photoreceptor neurons. Furthermore, electron microscopy, combined with stringent criteria for synapses, is the basis of connectomics. Further validation of our findings using both electrophysiological and electron microscopy methods is desirable.

We found behavioral adaptation of walking activity to the temperature at which the flies developed on the basis of a simple, multiparametric behavioral assay. It remains unclear to what extent this behavioral adaptation represents a fitness advantage. Similarly, how different developmental temperatures bring about such adaptive brain wiring remains a mystery.

STAR★METHODS

Detailed methods are provided in the online version of this paper and include the following:

- KEY RESOURCES TABLE
- RESOURCE AVAILABILITY
  - Lead contact
  - Materials availability
  - Data and code availability
- EXPERIMENTAL MODEL AND SUBJECT DETAILS
  - The following genotypes were used
- METHOD DETAILS
  - Immunohistochemistry and fixed imaging
  - Brain culture and live imaging
  - Trans-tango and activity-dependent GRASP
  - Electroretinogram (ERG) recordings
- QUANTIFICATION AND STATISTICAL ANALYSIS
  - Branch analysis (all neurons except adult motoneurons):
  - Branch analysis of adult motoneurons
  - Synapse number analysis:
  - Filopodia/axon branch tracing
  - Statistical analysis
  - Bulbous life time estimation
  - Buridan's paradigm object orientation assay
  - Measures of overall activity
  - Measures of movement angles or location independent of visual cue
  - Measures of angles or location relative to visual cue
  - Mathematical modeling
  - 'Developmental time' adjustment.
  - Parameter estimation

SUPPLEMENTAL INFORMATION

Supplemental information can be found online at https://doi.org/10.1016/j.celrep.2021.110145.

ACKNOWLEDGMENTS

We would like to thank Emil Kind, Mathias Wernet, Claude Desplan, and all members of the Hiesinger, Wernet, and Hassan labs for their support and helpful discussions. We thank Mathias Wernet, Claude Desplan, Michael Reiser, Stephan Sigrist, Gilad Barnea, Ian Meinertzhagen, the Janelia Research Institute, and the Bloomington *Drosophila* Stock Center for reagents. This work was supported by grants from the NIH (RO1EY018884) and the German Research Foundation (DFG; HI1886/5-1 and SFB186 TP02) to P.R.H. S.B.D. and B.A.H. were supported by an Einstein BIH Fellowship. C.D. was supported by the DFG (DU 331/12-1). M.v.K. acknowledges financial support from the German Ministry for Education and Science (BMBF) through grant 01KI2016 and from the DFG, provided through the excellence cluster Math+, project EF3-2.

AUTHOR CONTRIBUTIONS

Conceptualization, F.R.K. and P.R.H.; Methodology, F.R.K., S.B.D., S.H., C.P., G.A.L., and M.v.K.; Investigation, F.R.K., S.B.D., S.H., C.P., G.A.L., and

M.v.K.; Visualization, F.R.K., S.B.D., G.A.L., B.A.H., M.v.K., and P.R.H.; Funding Acquisition, B.A.H., M.v.K., and P.R.H.; Project Administration, P.R.H.; Supervision, P.R.H., B.A.H., C.D., and M.v.K.; Writing – Original Draft, F.R.K. and P.R.H.; Writing – Review & Editing, F.R.K., S.B.D., G.A.L., C.D., M.v.K., B.A.H., and P.R.H.

DECLARATION OF INTERESTS

The authors declare no competing interests.

Received: May 29, 2021
Revised: October 4, 2021
Accepted: November 29, 2021
Published: December 21, 2021

REFERENCES

Agi, E., Langen, M., Altschuler, S.J., Wu, L.F., Zimmermann, T., and Hiesinger, P.R. (2014). The evolution and development of neural superposition. J. Neurogenet. *28*, 216–232.

Agi, E., Kulkarni, A., and Hiesinger, P.R. (2020). Neuronal strategies for meeting the right partner during brain wiring. Curr. Opin. Neurobiol. *63*, 1–8.

Alonso, L.M., and Marder, E. (2020). Temperature compensation in a small rhythmic circuit. eLife *9*, e55470.

Bates, A.S., Schlegel, P., Roberts, R.J.V., Drummond, N., Tamimi, I.F.M., Turnbull, R., Zhao, X., Marin, E.C., Popovici, P.D., Dhawan, S., et al. (2020). Complete connectomic reconstruction of olfactory projection neurons in the fly brain. Curr. Biol. *30*, 3183–3199.e6.

Bekkers, J.M., and Stevens, C.F. (1991). Excitatory and inhibitory autaptic currents in isolated hippocampal neurons maintained in cell culture. Proc. Natl. Acad. Sci. U S A *88*, 7834–7838.

Carrillo, R.A., Özkan, E., Menon, K.P., Nagarkar-Jaiswal, S., Lee, P.T., Jeon, M., Birnbaum, M.E., Bellen, H.J., Garcia, K.C., and Zinn, K. (2015). Control of synaptic connectivity by a network of Drosophila IgSF cell surface proteins. Cell *163*, 1770–1782.

Cassidy, J.J., Bernasek, S.M., Bakker, R., Giri, R., Peláez, N., Eder, B., Bobrowska, A., Bagheri, N., Nunes Amaral, L.A., and Carthew, R.W. (2019). Repressive gene regulation synchronizes development with cellular metabolism. Cell *178*, 980–992.e17.

Clements, J., Lu, Z., Gehring, W.J., Meinertzhagen, I.A., and Callaerts, P. (2008). Central projections of photoreceptor axons originating from ectopic eyes in Drosophila. Proc. Natl. Acad. Sci. U S A *105*, 8968–8973.

Colomb, J., Reiter, L., Blaszkiewicz, J., Wessnitzer, J., and Brembs, B. (2012). Open source tracking and analysis of adult Drosophila locomotion in Buridan's paradigm with and without visual targets. PLoS ONE *7*, e42247.

Courgeon, M., and Desplan, C. (2019). Coordination between stochastic and deterministic specification in the *Drosophila* visual system. Science *366*, eaay6727.

Creed, J.H., Gerke, T.A., and Berglund, A.E. (2020). MatSurv: survival analysis and visualization in MATLAB. J. Open Source Softw. *5*, 1830.

de Wit, J., and Ghosh, A. (2016). Specification of synaptic connectivity by cell surface interactions. Nat. Rev. Neurosci. *17*, 22–35.

Douthit, J., Hairston, A., Lee, G., Morrison, C.A., Holguera, I., and Treisman, J.E. (2021). R7 photoreceptor axon targeting depends on the relative levels of *lost and found* expression in R7 and its synaptic partners. eLife *10*, e65895.

Duch, C., Vonhoff, F., and Ryglewski, S. (2008). Dendrite elongation and dendritic branching are affected separately by different forms of intrinsic motoneuron excitability. Journal of Neurophysiology (*100*), 2525–2536.

Dudanova, I., and Klein, R. (2013). Integration of guidance cues: parallel signaling and crosstalk. Trends Neurosci. *36*, 295–304.

Evers, J.F., Schmitt, S., Sibila, M., and Duch, C. (2005). Progress in functional neuroanatomy: precise automatic geometric reconstruction of neuronal morphology from confocal image stacks. J. Neurophysiol. *93*, 2331–2342.

Ferguson, M.W., and Joanen, T. (1982). Temperature of egg incubation determines sex in Alligator mississippiensis. Nature *296*, 850–853.

Fouquet, W., Owald, D., Wichmann, C., Mertel, S., Depner, H., Dyba, M., Hallermann, S., Kittel, R.J., Eimer, S., and Sigrist, S.J. (2009). Maturation of active zone assembly by Drosophila Bruchpilot. J. Cell Biol. *186*, 129–145.

Gilbert, S.F. (2012). Ecological developmental biology: environmental signals for normal animal development. Evol. Dev. *14*, 20–28.

Gillooly, J.F., Charnov, E.L., West, G.B., Savage, V.M., and Brown, J.H. (2002). Effects of size and temperature on developmental time. Nature *417*, 70–73.

Goaillard, J.M., and Marder, E. (2021). Ion channel degeneracy, variability, and covariation in neuron and circuit resilience. Annu. Rev. Neurosci. *44*, 335–357.

Goodman, C.S. (1978). Isogenic grasshoppers: genetic variability in the morphology of identified neurons. J. Comp. Neurol. *182*, 681–705.

Gutzke, W.H., and Crews, D. (1988). Embryonic temperature determines adult sexuality in a reptile. Nature *332*, 832–834.

Hadjieconomou, D., Timofeev, K., and Salecker, I. (2011). A step-by-step guide to visual circuit assembly in Drosophila. Curr. Opin. Neurobiol. *21*, 76–84.

Harris, J.M., Wang, A.Y., Boulanger-Weill, J., Santoriello, C., Foianini, S., Lichtman, J.W., Zon, L.I., and Arlotta, P. (2020). Long-range optogenetic control of axon guidance overcomes developmental boundaries and defects. Dev. Cell *53*, 577–588.e7.

Hassan, B.A., Bermingham, N.A., He, Y., Sun, Y., Jan, Y., Zoghbi, H.Y., and Bellen, H.J. (2000). *atonal* regulates neurite arborization but does not act as a proneural gene in the *Drosophila* brain. Neuron *25* (*3*), 549–561.

Hassan, B.A., and Hiesinger, P.R. (2015). Beyond molecular codes: simple rules to wire complex brains. Cell *163*, 285–291.

Hedgecock, E.M., and Russell, R.L. (1975). Normal and mutant thermotaxis in the nematode Caenorhabditis elegans. Proc. Natl. Acad. Sci. U S A *72*, 4061–4065.

Hertwig, O. (1898). Über den Einfluss der Temperatur auf die Entwicklung von Rana fusca und Rana esculenta. Archiv für Mikrosk. Anat. *51*, 319–382.

Hiesinger, P.R. (2021). Brain wiring with composite instructions. BioEssays *43*, e2000166.

Hiesinger, P.R., and Hassan, B.A. (2018). The evolution of variability and robustness in neural development. Trends Neurosci. *41*, 577–586.

Hiesinger, P.R., Zhai, R.G., Zhou, Y., Koh, T.W., Mehta, S.Q., Schulze, K.L., Cao, Y., Verstreken, P., Clandinin, T.R., Fischbach, K.F., et al. (2006). Activity-independent prespecification of synaptic partners in the visual map of Drosophila. Curr. Biol. *16*, 1835–1843.

Hoersting, A.K., and Schmucker, D. (2021). Axonal branch patterning and neuronal shape diversity: roles in developmental circuit assembly: Axonal branch patterning and neuronal shape diversity in developmental circuit assembly. Curr. Opin. Neurobiol. *66*, 158–165.

Hoge, M.A. (1915). Influence of temperature on the expression of a mendelian character. J. Exp. Zool. *18*, 241–286.

Karuppudurai, T., Lin, T.Y., Ting, C.Y., Pursley, R., Melnattur, K.V., Diao, F., White, B.H., Macpherson, L.J., Gallio, M., Pohida, T., and Lee, C.H. (2014). A hard-wired glutamatergic circuit pools and relays UV signals to mediate spectral preference in Drosophila. Neuron *81*, 603–615.

Kavalali, E.T., and Monteggia, L.M. (2020). Targeting homeostatic synaptic plasticity for treatment of mood disorders. Neuron *106*, 715–726.

Kidd, P.B., Young, M.W., and Siggia, E.D. (2015). Temperature compensation and temperature sensation in the circadian clock. Proc. Natl. Acad. Sci. U S A *112*, E6284–E6292.

Kiral, F.R., Linneweber, G.A., Mathejczyk, T., Georgiev, S.V., Wernet, M.F., Hassan, B.A., von Kleist, M., and Hiesinger, P.R. (2020). Autophagy-dependent filopodial kinetics restrict synaptic partner choice during Drosophila brain wiring. Nat. Commun. *11*, 1325.

Kohrs, F.E., Daumann, I.M., Pavlovic, B., Jin, E.J., Kiral, F.R., Lin, S.C., Port, F., Wolfenberg, H., Mathejczyk, T.F., Linneweber, G.A., et al. (2021). Systematic

functional analysis of rab GTPases reveals limits of neuronal robustness to environmental challenges in flies. eLife *10*, e59594.

Kolodkin, A.L., and Hiesinger, P.R. (2017). Wiring visual systems: common and divergent mechanisms and principles. Curr. Opin. Neurobiol. *42*, 128–135.

Kuntz, S.G., and Eisen, M.B. (2014). Drosophila embryogenesis scales uniformly across temperature in developmentally diverse species. PLoS Genet. *10*, e1004293.

Kushinsky, D., Morozova, E.O., and Marder, E. (2019). *In vivo* effects of temperature on the heart and pyloric rhythms in the crab *Cancer borealis*. J. Exp. Biol. *222*, jeb199190.

Langen, M., Agi, E., Altschuler, D.J., Wu, L.F., Altschuler, S.J., and Hiesinger, P.R. (2015). The developmental rules of neural superposition in Drosophila. Cell *162*, 120–133.

Langen, M., Koch, M., Yan, J., De Geest, N., Erfurth, M.L., Pfeiffer, B.D., Schmucker, D., Moreau, Y., and Hassan, B.A. (2013). Mutual inhibition among postmitotic neurons regulates robustness of brain wiring in *Drosophila*. eLife *2* (*e00337*).

Li, F., Lindsey, J.W., Marin, E.C., Otto, N., Dreher, M., Dempsey, G., Stark, I., Bates, A.S., Pleijzier, M.W., Schlegel, P., et al. (2020). The connectome of the adult Drosophila mushroom body provides insights into function. eLife *9*, e62576.

Lieberman, O.J., McGuirt, A.F., Tang, G., and Sulzer, D. (2019). Roles for neuronal and glial autophagy in synaptic pruning during development. Neurobiol. Dis. *122*, 49–63.

Linneweber, G.A., Andriatsilavo, M., Dutta, S.B., Bengochea, M., Hellbruegge, L., Liu, G., Ejsmont, R.K., Straw, A.D., Wernet, M., Hiesinger, P.R., and Hassan, B.A. (2020). A neurodevelopmental origin of behavioral individuality in the *Drosophila* visual system. Science *367*, 1112–1119.

Luo, J., Ting, C.Y., Li, Y., McQueen, P., Lin, T.Y., Hsu, C.P., and Lee, C.H. (2020). Antagonistic regulation by insulin-like peptide and activin ensures the elaboration of appropriate dendritic field sizes of amacrine neurons. eLife *9*, e50568.

Macpherson, L.J., Zaharieva, E.E., Kearney, P.J., Alpert, M.H., Lin, T.Y., Turan, Z., Lee, C.H., and Gallio, M. (2015). Dynamic labelling of neural connections in multiple colours by trans-synaptic fluorescence complementation. Nat. Commun. *6*, 10024.

Menon, K.P., Kulkarni, V., Takemura, S.Y., Anaya, M., and Zinn, K. (2019). Interactions between Dpr11 and DIP-γ control selection of amacrine neurons in *Drosophila* color vision circuits. eLife *8*, e48935.

Namiki, S., Dickinson, M.H., Wong, A.M., Korff, W., and Card, G.M. (2018). The functional organization of descending sensory-motor pathways in *Drosophila*. eLife *7*, e34272.

O'Leary, T., and Marder, E. (2016). Temperature-robust neural function from activity-dependent ion channel regulation. Curr. Biol. *26*, 2935–2941.

Özel, M.N., Langen, M., Hassan, B.A., and Hiesinger, P.R. (2015). Filopodial dynamics and growth cone stabilization in Drosophila visual circuit development. eLife *4*, e10721.

Özel, M.N., Kulkarni, A., Hasan, A., Brummer, J., Moldenhauer, M., Daumann, I.M., Wolfenberg, H., Dercksen, V.J., Kiral, F.R., Weiser, M., et al. (2019). Serial synapse formation through filopodial competition for synaptic seeding factors. Dev. Cell *50*, 447–461.e8.

Pak, W.L., Grossfield, J., and White, N.V. (1969). Nonphototactic mutants in a study of vision of Drosophila. Nature *222*, 351–354.

Petrovic, M., and Schmucker, D. (2015). Axonal wiring in neural development: target-independent mechanisms help to establish precision and complexity. BioEssays *37*, 996–1004.

Rajpurohit, S., and Schmidt, P.S. (2016). Measuring thermal behavior in smaller insects: a case study in Drosophila melanogaster demonstrates effects of sex, geographic origin, and rearing temperature on adult behavior. Fly (Austin) *10*, 149–161.

Rister, J., Desplan, C., and Vasiliauskas, D. (2013). Establishing and maintaining gene expression patterns: insights from sensory receptor patterning. Development *140*, 493–503.

Roberts, E. (1918). Fluctuation in a recessive mendelian character. J. Exp. Zool. *27*, 157–192.

Ryglewski, S., Vonhoff, F., Scheckel, K., and Duch, C. (2017). Intra-neuronal competition for synaptic partners conserves the amount of dendritic building material. Neuron *93*, 632–645.e6.

Sanes, J.R., and Zipursky, S.L. (2020). Synaptic specificity, recognition molecules, and assembly of neural circuits. Cell *181*, 536–556.

Scheffer, L.K., Xu, C.S., Januszewski, M., Lu, Z., Takemura, S.Y., Hayworth, K.J., Huang, G.B., Shinomiya, K., Maitlin-Shepard, J., Berg, S., et al. (2020). A connectome and analysis of the adult *Drosophila* central brain. eLife *9*, e57443.

Schmitt, S., Evers, J.F., Duch, C., Scholz, M., and Obermayer, K. (2004). New methods for the computer-assisted 3D reconstruction of neurons from confocal image stacks. Neuroimage *23*, 1283–1298.

Seyster, E.W. (1919). Eye facet number as influenced by temperature in the bar-eyed mutatn of Drosophila. Biol. Bull. *37*, 168–181.

Shatz, C.J. (1996). Emergence of order in visual system development. Proc. Natl. Acad. Sci. U S A *93*, 602–608.

Südhof, T.C. (2018). Towards an understanding of synapse formation. Neuron *100*, 276–293.

Takemura, S.Y., Xu, C.S., Lu, Z., Rivlin, P.K., Parag, T., Olbris, D.J., Plaza, S., Zhao, T., Katz, W.T., Umayam, L., et al. (2015). Synaptic circuits and their variations within different columns in the visual system of Drosophila. Proc. Natl. Acad. Sci. U S A *112*, 13711–13716.

Talay, M., Richman, E.B., Snell, N.J., Hartmann, G.G., Fisher, J.D., Sorkaç, A., Santoyo, J.F., Chou-Freed, C., Nair, N., Johnson, M., et al. (2017). Transsynaptic mapping of second-order taste neurons in flies by *trans*-Tango. Neuron *96*, 783–795.e4.

Trush, O., Liu, C., Han, X., Nakai, Y., Takayama, R., Murakawa, H., Carrillo, J.A., Takechi, H., Hakeda-Suzuki, S., Suzuki, T., and Sato, M. (2019). N-cadherin orchestrates self-organization of neurons within a columnar unit in the *Drosophila* medulla. J. Neurosci. *39*, 5861–5880.

Turrigiano, G. (2012). Homeostatic synaptic plasticity: local and global mechanisms for stabilizing neuronal function. Cold Spring Harb. Perspect. Biol. *4*, a005736.

Turrigiano, G.G. (2017). The dialectic of Hebb and homeostasis. Philos. Trans. R. Soc. Lond. B Biol. Sci. *372*, 20160258.

Van der Loos, H., and Glaser, E.M. (1972). Autapses in neocortex cerebri: synapses between a pyramidal cell's axon and its own dendrites. Brain Res. *48*, 355–360.

Vonhoff, F., and Duch, C. (2010). Tiling among stereotyped dendritic branches in an identified Drosophila motoneuron. J. Comp. Neurol. *518*, 2169–2185.

Wilton, D.K., Dissing-Olesen, L., and Stevens, B. (2019). Neuron-glia signaling in synapse elimination. Annu. Rev. Neurosci. *42*, 107–127.

Witvliet, D., Mulcahy, B., Mitchell, J.K., Meirovitch, Y., Berger, D.R., Wu, Y., Liu, Y., Koh, W.X., Parvathala, R., Holmyard, D., et al. (2021). Connectomes across development reveal principles of brain maturation. Nature *596*, 257–261.

Xu, S., Xiao, Q., Cosmanescu, F., Sergeeva, A.P., Yoo, J., Lin, Y., Katsamba, P.S., Ahlsen, G., Kaufman, J., Linaval, N.T., et al. (2018). Interactions between the Ig-superfamily proteins DIP-α and Dpr6/10 regulate assembly of neural circuits. Neuron *100*, 1369–1384.e6.

Zuo, W., Moses, M.E., West, G.B., Hou, C., and Brown, J.H. (2012). A general model for effects of temperature on ectotherm ontogenetic growth and development. Proc. Biol. Sci. *279*, 1840–1846.

STAR★METHODS

KEY RESOURCES TABLE

REAGENT or RESOURCE	SOURCE	IDENTIFIER
Antibodies		
Rat anti-Cadherin, DN (extracellular domain)	DSHB	Cat# DN-Ex #8; RRID: AB 528121
Goat anti-GFP pAb	Abcam	Cat# ab6673; RRID: AB 305643
Rat anti-GFP mAb	BioLegend	Cat# 338002; RRID: AB 1279414
Rabbit anti-CD4	Atlas Antibodies	Cat# HPA004252; RRID:AB 1078466
Rabbit anti-dsRed	Takara Bio	Cat# 632496; RRID: AB 10013483
Donkey anti-goat Alexa Fluor 488	Jackson ImmunoResearch Labs	Cat# 705-545-147; RRID: AB 2336933
Donkey Anti-goat Cy5	Jackson ImmunoResearch Labs	Cat# 705-175-147; RRID: AB 2340415
Donkey Anti-rabbit Cy3	Jackson ImmunoResearch Labs	Cat# 711-165-152; RRID: AB 2307443
Donkey Anti-rat Cy5	Jackson ImmunoResearch Labs	Cat# 112-175-143; RRID: AB 2338263
Chemicals, peptides, and recombinant proteins		
Vectashield	Vector Laboratories	H-1000
PBS	GIBCO	70011-36
Formaldehyde	Merck KGaA	1.03999.1000
Triton X-100	Sigma-Aldrich	T8787
Schneider's *Drosophila* Medium [+] L-Glutamine	GIBCO	21720-024
Agarose, low gelling temperature	Sigma-Aldrich	A9045-10G
Human insulin recombinant zinc	GIBCO	12585014
Penicillin/Streptomycin	GIBCO	15140122
ES Cell FBS	GIBCO	16141-061
20-Hydroxyecdysone	Sigma-Aldrich	5289-74-7
SilGard and Silicone Elastomer Kit	Dow Corning	184
Sodium Chloride	Merck KGaA	1.06404.1000
Experimental models: Organisms/strains		
Drosophila: UAS-brpD3::GFP	Gift from S.Sigrist	N/A
Drosophila: UAS-myr::GFP,QUAS-mtdTomato(3xHA)	Bloomington Drosophila Stock Center	RRID: BDSC_77479
Drosophila: trans-Tango	Bloomington Drosophila Stock Center	RRID: BDSC_77123
Drosophila: DIPγ^{null}	Gift from C.Desplan	N/A
Drosophila: Rh4-Gal4	Gift from M.Wernet	N/A
Drosophila: Rh4-LacZ	Gift from M.Wernet	N/A
Drosophila: R48A07-p65ADZp(attP40), R79H02-ZpGdbd(attP2)	Gift from M.Reiser	N/A
Drosophila: Lawf1-Gal4	Gift from M.Reiser	N/A
Drosophila: ato-Gal4-14a	Hassan et al., 2000	https://doi.org/10.1016/S0896-6273(00)81059-4
Drosophila: ato-LexA	Langen et al., 2013	https://doi.org/10.7554/eLife.00337
Drosophila: UAS-nSyb-spGFP1-10,lexAop-CD4-spGFP	Bloomington Drosophila Stock Center	RRID: BDSC_64314
Drosophila: lexAop-nSyb-spGFP1-10,UAS-CD4-spGFP11	Bloomington Drosophila Stock Center	RRID: BDSC_64315
Drosophila: hsFLP	Bloomington Drosophila Stock Center	RRID: BDSC_8862
Drosophila: GMR-Gal4	Bloomington Drosophila Stock Center	RRID: BDSC_8121
Drosophila: GMR-Flp	Bloomington Drosophila Stock Center	RRID: BDSC_42735

(*Continued on next page*)

Continued

REAGENT or RESOURCE	SOURCE	IDENTIFIER
Drosophila: FRT82B, tub-Gal80	Bloomington Drosophila Stock Center	RRID: BDSC_5135
Drosophila: lexAop-mCD8::GFP	Bloomington Drosophila Stock Center	RRID: BDSC_32203
Drosophila: UAS-mCD4::tdGFP	Bloomington Drosophila Stock Center	RRID:BDSC_35836
Drosophila: UAS-mCD4::tdTomato	Bloomington Drosophila Stock Center	RRID:BDSC_35837
Drosophila: GMR49B06-LexA	Bloomington Drosophila Stock Center	RRID:BDSC_52707
Drosophila: GMR19F01-LexA	Bloomington Drosophila Stock Center	RRID:BDSC_52547
Drosophila: GMR25F10-LexA	Bloomington Drosophila Stock Center	RRID:BDSC_54603
Drosophila: GMR42H01-LexA	Bloomington Drosophila Stock Center	RRID:BDSC_54204
Drosophila: GMR20D11-LexA	Bloomington Drosophila Stock Center	RRID:BDSC_52565
Drosophila: GMR38H06-LexA	Bloomington Drosophila Stock Center	RRID:BDSC_52775
Drosophila: GMR11C05-LexA	Bloomington Drosophila Stock Center	RRID:BDSC_54608
Drosophila: ortC1-3-LexADBD, ortC2B-dVP16AD	Gift from M.Wernet	N/A
Drosophila: GMR24F06-Gal4	Bloomington Drosophila Stock Center	RRID: BDSC_49087
Software and algorithms		
GraphPad Prism	GraphPad Software	RRID: SCR_002798
ImageJ	National Institutes of Health (NIH)	RRID: SCR_002285
IMARIS	Bitplane AG	RRID: SCR_007370
Leica Application Suite X	Leica Microsystems	RRID: SCR_013673
Clampfit	Axon Instruments	RRID: SCR_011323
Clampex	Axon Instruments	RRID: SCR_011323
Amira	FEI-Thermo Fisher Scientific	RRID: SCR_014305
Custom code	Zenodo	https://doi.org/10.5281/zenodo.5708543

RESOURCE AVAILABILITY

Lead contact

Further information and requests for resources and reagents should be directed to and will be fulfilled by the lead contact, P. Robin Hiesinger (robin.hiesinger@fu-berlin.de).

Materials availability

All reagents and resources generated in this study are available from the Lead Contact without restriction..

Data and code availability

All data generated in this study are available from the Lead Contact without restriction.

A publication release of original code has been generated and deposited on Zenodo and is publicly available under https://doi.org/10.5281/zenodo.5708543.

Any additional information required to reanalyze the data reported in this work paper is available from the Lead Contact upon request.

EXPERIMENTAL MODEL AND SUBJECT DETAILS

Flies were reared at 25°C on standard cornmeal/yeast diet unless stated otherwise. For developmental analyses white pre-pupae (P+0%) were collected and staged to pupal developmental stages shown on figures. The following *Drosophila* strains were either obtained from Bloomington *Drosophila* Stock Center (BDSC) or other groups: UAS-Brp-short-GFP (S.Sigrist); Trans-tango flies (G.Barnea); DIPγ^{null} (C.Desplan); Rh4-Gal4, Rh4-LacZ (M.Wernet); R48A07-p65ADZp(attP40); R79H02-ZpGdbd(attP2) (Mi4-specific split Gal4 driver), Lawf1-Gal4 (M.Reiser); ato-Gal4-14a, ato-LexA, GRASP flies, hsflp, GMRflp, GMR-Gal4, GMR(FRT.stop)Gal4, FRT82B, GMR-Gal80, tub-Gal80, LexAop-CD8-GFP, UAS-CD4-tdGFP, UAS(FRT.stop)CD4-tdGFP, UAS-CD4-tdTomato, GMRmyr-tomato, GMR49B06-LexA (Mi4-specific driver), GMR19F01-LexA (Mi1-specific driver), GMR25F10-LexA (Tm9-specific driver), GMR42H01-LexA (Dm9-specific driver), GMR20D11-LexA (Dm3-specific driver), GMR38H06-LexA (Dm6-specific driver), GMR11C05-LexA (Dm11-specific driver), ortC1-3-LexADBD, ortC2B-dVP16AD (Dm8-specific driver), GMR24F06-Gal4 (Dm8-specific

driver), R14F03-p65ADZp, R24C07-ZpGdbd (DNp24- specific split-Gal4 driver) (BDSC). Flies of both sexes were equally used in all experiments unless otherwise noted in the paper.

The following genotypes were used

Figures 1B–1E: GMRflp; GMR-Gal4, UAS-CD4tdGFP; FRT82B, tub-Gal80/FRT82B
Figures 1I–1L: GMRflp; GMR-Gal4, UAS-CD4tdTomato/UAS-Brp^{short}-GFP; FRT82B, tub-Gal80/FRT82B
Figures 2A–2D: UAS-myrGFP, QUAS-mtdTomato(3xHA); Rh4-Gal4/*trans*-Tango
Figure 2E: Rh4-Gal4, UAS-nsyb::splitGFP1-10, LexAop-splitGFP11/ ortC1-3-LexADBD, ortC2B-dVP16AD (Dm8-specific driver)
Figure 2F: Rh4-Gal4, UAS-nsyb::splitGFP1-10, LexAop-splitGFP11/GMR19F01-LexA (Mi1-specific driver)
Figure 2G: Rh4-Gal4, UAS-nsyb::splitGFP1-10, LexAop-splitGFP11/GMR49B06-LexA (Mi4-specific driver)
Figure 2H: Rh4-Gal4, UAS-nsyb::splitGFP1-10, LexAop-splitGFP11/GMR25F10-LexA (Tm9-specific driver)
Figures 3A and 3A′: Rh4-Gal4, UAS-nsyb::splitGFP1-10, LexAop-splitGFP11/ortC1-3-LexADBD, ortC2B-dVP16AD (Dm8-specific driver); *DIP*γ^{null}/+
Figures 3B and 3B′: Rh4-Gal4, UAS-nsyb::splitGFP1-10, LexAop-splitGFP11/ortC1-3-LexADBD, ortC2B-dVP16AD (Dm8-specific driver); *DIP*γ^{null}/ *DIP*γ^{null}
Figures 3D and 3D′: Rh4-Gal4/ UAS-Brp^{short}-GFP; *DIP*γ^{null}/+
Figures 3E and 3E′: Rh4-Gal4/ UAS-Brp^{short}-GFP; *DIP*γ^{null}/ *DIP*γ^{null}
Figure 3G: UAS-myrGFP, QUAS-mtdTomato(3xHA); Rh4-Gal4/*trans*-Tango; *DIP*γ^{null}/+
Figure 3H: UAS-myrGFP, QUAS-mtdTomato(3xHA); Rh4-Gal4/*trans*-Tango; *DIP*γ^{null}/ *DIP*γ^{null}
Figure 3J: Rh4-Gal4, UAS-nsyb::splitGFP1-10, LexAop-splitGFP11/ GMR19F01-LexA (Mi1-specific driver); *DIP*γ^{null}/+ and *DIP*γ^{null}/ *DIP*γ^{null}
Figure 3K: Rh4-Gal4, UAS-nsyb::splitGFP1-10, LexAop-splitGFP11/GMR49B06-LexA (Mi4-specific driver); *DIP*γ^{null}/+ and *DIP*γ^{null}/ *DIP*γ^{null}
Figure 3L: Rh4-Gal4, UAS-nsyb::splitGFP1-10, LexAop-splitGFP11/ GMR25F10-LexA (Tm9-specific driver); *DIP*γ^{null}/+ and *DIP*γ^{null}/ *DIP*γ^{null}
Figure 4A: GMRflp; GMR-Gal4, UAS-CD4tdTomato/UAS-Brp^{short}-GFP; FRT82B, tub-Gal80/FRT82B
Figures 4B and 4C: Canton-S WT flies
Figures 4D–4G: hsflp; UAS(FRT.stop)CD4tdGFP; GMR24F06-Gal4 (Dm8-specific driver)
Figures 4H–4J: hsflp; UAS(FRT.stop)CD4tdGFP/ R48A07-p65ADZp(attP40); R79H02-ZpGdbd(attP2) (Mi4-specific split Gal4 driver)
Figures 5B–5G: ;UAS-CD4tdGFP/+;Ato-Gal4,UAS-CD4tdGFP/+
Figures 5H–5J: ;UAS-Brp^{short}-GFP/+;Ato-Gal4,UAS-CD4tdTomato/+
Figures 5K–5M: UAS-myrGFP, QUAS-mtdTomato(3xHA); *trans*-Tango/+;Ato-Gal4/+
Figures 5N–5P′: ;LexAop-nsyb::splitGFP1-10, UAS-splitGFP11/R52H01AD;Ato-LexA/R19C10DBD (Lawf1 split Gal4)
Figure 6: Canton-S WT flies (used in *(12)* to perform EM connectome analysis of synaptic partners in the *Drosophila* visual system)
Figure S1B: UAS-myrGFP, QUAS-mtdTomato(3xHA); Rh4-Gal4/*trans*-Tango
Figure S1C: UAS-myrGFP, QUAS-mtdTomato(3xHA); Rh4-Gal4/*trans*-Tango; *DIP*γ^{null}/ *DIP*γ^{null}
Figure S2: UAS-myrGFP, QUAS-mtdTomato(3xHA); Rh4-Gal4/*trans*-Tango
Figure S3: Rh4-Gal4, UAS-nsyb::splitGFP1-10, LexAop-splitGFP11/ ortC1-3-LexADBD, ortC2B-dVP16AD (Dm8-specific driver)
Figures S4A–S4C: ortC1-3-LexADBD, ortC2B-dVP16AD (Dm8-specific driver), LexAop-CD8GFP
Figures S4D and S4D′: ortC1-3-LexADBD, ortC2B-dVP16AD (Dm8-specific driver), LexAop-CD8GFP/Rh4-LacZ; *DIP*γ^{null}/+
Figures S4E and S4E′: ortC1-3-LexADBD, ortC2B-dVP16AD (Dm8-specific driver), LexAop-CD8GFP/Rh4-LacZ; *DIP*γ^{null}/ *DIP*γ^{null}
Figures S4F and S4G: UAS-myrGFP, QUAS-mtdTomato(3xHA); Rh4-Gal4/*trans*-Tango; *DIP*γ^{null}/ *DIP*γ^{null}
Figures S5B and S5B′: Rh4-Gal4, UAS-nsyb::splitGFP1-10, LexAop-splitGFP11/GMR42H01-LexA (Dm9-specific driver); *DIP*γ^{null}/+
Figures S5C and S5C′: Rh4-Gal4, UAS-nsyb::splitGFP1-10, LexAop-splitGFP11/GMR42H01-LexA (Dm9-specific driver); *DIP*γ^{null}/ *DIP*γ^{null}
Figures S5E and S5E′: Rh4-Gal4, UAS-nsyb::splitGFP1-10, LexAop-splitGFP11/GMR11C05-LexA (Dm11-specific driver); *DIP*γ^{null}/+
Figures S5F and S5F′: Rh4-Gal4, UAS-nsyb::splitGFP1-10, LexAop-splitGFP11/GMR11C05-LexA (Dm11-specific driver); *DIP*γ^{null}/ *DIP*γ^{null}
Figures S5H and S5H′: Rh4-Gal4, UAS-nsyb::splitGFP1-10, LexAop-splitGFP11/GMR20D11-LexA (Dm3-specific driver); *DIP*γ^{null}/+
Figures S5I and S5I′: Rh4-Gal4, UAS-nsyb::splitGFP1-10, LexAop-splitGFP11/GMR20D11-LexA (Dm3-specific driver); *DIP*γ^{null}/ *DIP*γ^{null}
Figures S5J and S5J′: Rh4-Gal4, UAS-nsyb::splitGFP1-10, LexAop-splitGFP11/ GMR38H06-LexA (Dm6-specific driver); *DIP*γ^{null}/+

Figures S5K and S5K′: Rh4-Gal4, UAS-nsyb::splitGFP1-10, LexAop-splitGFP11/ GMR38H06-LexA (Dm6-specific driver); $DIP\gamma^{null}$/ $DIP\gamma^{null}$
Figures S6A–S6D: GMRflp; GMR-Gal4, UAS-CD4tdTomato/UAS-Brp^{short}-GFP; FRT82B, tub-Gal80/FRT82B
Figures S6E–S6G: Canton-S WT flies
Figures S6H–S6J: hsflp; UAS(FRT.stop)CD4tdGFP; GMR24F06-Gal4 (Dm8-specific driver)
Figure S7: R14F03-p65ADZp, R24C07-ZpGdbd (DNp24- specific split-Gal4 driver); UAS-CD4tdGFP
Figure S8: GMR23H06-ADZ attP40/UAS-cd4-tdGFP;GMR30A07-DBD attP2/+
Figure S9: UAS-myrGFP, QUAS-mtdTomato(3xHA); *trans*-Tango/+;Ato-Gal4/+
Figures S10–S12: Canton-S WT flies

METHOD DETAILS

Immunohistochemistry and fixed imaging

Pupal and adult eye-brain complexes were dissected in cold Schneider's *Drosophila* medium and fixed in 4% paraformaldehyde (PFA) in PBS for 40 minutes. Tissues were washed in PBST (0.4% Triton-X) and mounted in Vectashield (Vector Laboratories, CA). Images were obtained with a Leica TCS SP8-X white laser confocal microscope with a 63X glycerol objective (NA = 1.3). The primary antibodies used in this study with given dilutions were as follows: rat monoclonal anti-nCadherin (1:100; Developmental Studies Hybridoma Bank); goat polyclonal anti-GFP (1:1000; Abcam); rat monoclonal anti-GFP (1:500; BioLegend); rabbit polyclonal anti-CD4 (1:600; Atlas Antibodies); rabbit polyclonal anti-DsRed (1:500; ClonTech). The secondary antibodies Alexa488, Cy3, Cy5 (Jackson ImmunoResearch Laboratories) were used in 1:500 dilution.

Brain culture and live imaging

For all *ex vivo* live imaging experiments an imaging window cut open removing posterior head cuticle partially. The resultant eye-brain complexes were mounted in 0.4% dialyzed low-melting agarose in a modified culture medium. Live imaging was performed using a Leica SP8 MP microscope with a 40X IRAPO water objective (NA = 1.1) with a Chameleon Ti:Sapphire laser and Optical Parametric Oscillator (Coherent). The excitation laser was set to 900 nm for single channel CD4-tdGFP imaging. Live imaging of R7 axon terminals at different temperatures was performed as follows: white pre-pupae (P+0%) were collected and staged to P+60% at 25°C. After eye-brain complexes were mounted in 0.4% dialyzed low-melting agarose in a modified culture medium, they were incubated 1 hour in imaging chamber at given temperatures on figures and scanned live for another hour with 1-min time resolution at the same incubation temperature. The same experimental flow and imaging settings were used for live imaging of Dorsal cluster neuron (DCN) axonal branches except that live imaging was performed at P+50%.

Trans-tango and activity-dependent GRASP

Trans-tango and GRASP experiments were performed with yellow R7-specific driver Rh4-Gal4 and DCN-specific ato-Gal4-14a. Trans-tango flies were raised at 25°C until P+40% and moved to 18°C or 29°C for temperature shift experiments. On the day of eclosion, flies were transferred back to 25°C and dissected after 1 week. The number of postsynaptic neurons was counted manually from their cell bodies using cell counter plugin in Fiji including all cell bodies with weak or strong labeling to reveal all potential connections. Since postsynaptic partner labeling by Trans-tango is age-dependent, in another set of experiments, 1-day old flies were dissected to reveal the identity of cell types strongly connected to DCNs. For activity-dependent GRASP experiments, the same experimental flow was followed as in Trans-tango temperature shift experiments. To activate UV-sensitive R7-photoreceptors, flies were transferred to UV-transparent Plexiglas vials on the day of eclosion and kept in a custom-made light box with UV light (25°C, 20-4 light-dark cycle) for 4 days. To activate DCNs, flies were transferred to 25°C incubator with 12-12 light-dark cycle for 5 days. Brains were dissected and stained with a polyclonal anti-GFP antibody to label R7 photoreceptors, monoclonal anti-GFP antibody to label GRASP signal, and polyclonal anti-CD4 antibody to label postsynaptic neurons.

Electroretinogram (ERG) recordings

Newly-hatched (0-day old) adult flies were collected and glued on slides using nontoxic school glue. Flies were exposed to alternating 1 s "on" 2 s "off" light stimulus provided by computer-controlled white LED system (MC1500; Schott). ERGs were recorded using Clampex (Axon Instruments) and quantified using Clampfit (Axon Instruments).

QUANTIFICATION AND STATISTICAL ANALYSIS

Branch analysis (all neurons except adult motoneurons):

All imaging data were analyzed and presented with Imaris 9.0.1 (Bitplane). Branches were detected automatically with the filament module using identical parameters for all experimental conditions (largest dendrite diameter: 3.0 μm, thinnest dendrite diameter: 0.2 μm). Inconsistencies in automatic detection were checked and corrected manually. The resultant values of branch numbers and lengths were taken and recorded directly from the statistics tab of the filament module. The peripheral area of the branch arborization was marked manually with the Surface function using the same mode for all experimental conditions (selection mode: isoclick)

and a consequent surface was generated for the entire branching area marked manually. The resultant values of surface area were taken and recorded directly from the statistics tab of the surface module. Graph generation and statistical analyses were done using GraphPad Prism 8.2.0

Branch analysis of adult motoneurons

For analysis of motoneuron dendritic structure *Drosophila melanogaster* were reared at 25°C, on a 12/12hrs light/dark cycle, in plastic vials on a cornmeal, glucose, yeast, agar diet (for 6 l: 725.69 g glucose, 343.06 g cornmeal, 66 g Agar and 181.38 g active dry yeast; after cooling to 70°C 76.25 mL Tegosept (10% in 100% ethanol) were added. Ascorbic acid was added (3.5 g) after cooling to 65°C. For all experiments male flies that express cd4-tdGFP in DLM flight motoneurons were used (genotype: w;GMR23H06-ADZ attP40/UAS-cd4-tdGFP;GMR30A07-DBD attP2/+). To test for effects of temperature on dendritic differentiation of DLM flight motoneurons, animals were raised at 25°C from egg to late third instar larva and transferred at the prepupal stage to either 18°C, or 29°C, or kept at 25°C. After adult eclosion, all animals were transferred to 25°C. For each temperature protocol in 5 male animals one MN was stained intracellularly at the second day of adult life. Adult DLM flight motoneurons were filled as previously described (Duch et al., 2008; Ryglewski et al., 2017). Confocal image stacks were acquired with a Leica TSC SP8 confocal laser scanning microscope with a 40x, 1.25 NA oil lens at a zoom of 3.5. Excitation wavelength was 561 nm (DPSS laser) and PMT detection between 570 and 600 nm. Voxel dimensions were 86 × 86 × 300 nm (x, y, z). Image stacks were imported into Amira software (AMIRA 4.1.1, FEI, Hillsboro, Oregon, US) and dendritic structure reconstructions were conducted with custom plug-ins as previously described (Schmitt et al., 2004; Evers et al., 2005). As metric parameters the number of dendritic branches, total dendritic length (TDL), the mean length of all dendritic branches (MDL), and the mean radius of all dendritic branches (MDR) were readout. For branch order analysis, the entire neurite from the cell body to the axon leaving the ventral nerve cord was defined as tree origin and thus branch order 0. All dendrites that directly branch off that neurite were first order branches, all dendrites branching off first order branches were second order branches and so on. The number of dendrites in each branch order was counted for each temperature condition.

Synapse number analysis:

All imaging data were analyzed and presented with Imaris 9.0.1 (Bitplane). For synapse number analysis, CD4-tomato channel was used to generate surfaces for individual R7 axon terminals and DCN axonal branches. Brp-positive puncta inside the surface were filtered using the masking function and were automatically detected with the spot detection module (spot diameter was set to 0.3 μ). Synapse numbers were taken and recorded directly from the statistics tab of the spot function. To obtain synapse density, the number of Brp-positive puncta inside individual DCN branch was divided by the respective branch length. Graph generation and statistical analyses were done using GraphPad Prism 8.2.0

Filopodia/axon branch tracing

Filopodia/axon branch tracing was performed using the filament module of Imaris 9.0.1 (BitPlane). Each filopodia/axon branch for all time points was segmented manually using ''automatic placement'' option to ensure the measurement of actual 3D length of each filopodia/axonal branch. Node was defined by the junction of axon shaft-branching point, from which filaments were created covering the entire length of the respective branch for all time points. ''Length over time'' data for all segmented filopodia/axon branch were recorded directly from the statistics tab of the filament module to calculate speed. Graph generation and statistical analyses were done using GraphPad Prism 8.2.0.

Statistical analysis

Statistical comparison of two groups was performed with non-parametric Kolmogorov-Smirnov test. Statistical comparison of more than two groups was performed with non-parametric Kruskal-Wallis test and corrected for multiple comparisons with Dunn's as a post hoc test. All significance values are denoted on the graphs and in their respective legends. Graph generation and statistical analyses were done using GraphPad Prism 8.2.0.

Bulbous life time estimation

We used the Kaplan-Meier estimator provided in MatSurv (Creed et al., 2020) to estimate the Bulbous tip survival probability depicted in Figure 1F.

Buridan's paradigm object orientation assay

Fly object orientation behavior was tested according to standard protocols in a Buridan arena (Colomb et al., 2012; Linneweber et al., 2020) using flies grown in a 12/12 h light–dark cycle. The arena consisted of a round platform of 117 mm in diameter, surrounded by a water-filled moat and placed inside a uniformly illuminated white cylinder. The assay was lid using four circular fluorescent tubes (Osram, L 40w, 640 C circular cool white) powered by an Osram Quicktronic QT-M 1 × 26–42. The fluorescent tubes were located outside of a diffuser (DeBanier, Belgium, 2090051, Kalk transparent, 180 g, white) positioned 147.5 mm from the arena center. The temperature on the platform was 25 °C and 30 mm-wide stripes of black cardboard were placed on opposing sides inside of the diffuser. The retinal size of the stripes depended on the position of the fly on the platform and ranged from 8.4° to 19.6° in width (11.7° in the center of the platform). Fly tracks were analyzed using CeTrAn (Colomb et al., 2012) and custom-written python code

(Linneweber et al., 2020). We evaluated 44 partially overlapping behavioral parameters and have picked 25 representative from these for detailed analysis as shown in Figure 6 and Figure S8 and Table S2. The behavioral parameters are the following (Colomb et al., 2012; Linneweber et al., 2020):

Measures of overall activity

1. **Number of walks:** The number of times a fly walks from one stripe to the other. The fly needs to be on both ends near the edge more than 80% of the platform radius.
2. **Pause duration (s):** Median duration of pauses in seconds
3. **Distance traveled (mm/min):** Total distance traveled per minute.
4. **Relative time moving:** ratio of moving versus not moving over the entire length of the fly track.
5. **Activity time (s):** Time active per minute in seconds
6. **Speed (mm/s):** Division of the distance traveled by time in mm/s. The reported value is the median speed of each fly. Movements exceeding 50mm/s are excluded in the median speed calculation.
7. **Number of pauses:** number of pauses per minute.
8. **Activity bouts (s):** Median duration of bouts of activity in seconds

Measures of movement angles or location independent of visual cue

9. **Meandering (degrees/mm):** Measurement of the tortuosity (twistedness) of the track, calculated as Turning Angle divided by the speed. Shown as median value in degrees/mm.
10. **Turning angle (degrees)**: Median angle of all turns a fly does in the arena.
11. **Centrophobism while moving:** The arena is divided in an inner and outer ring of equal size. The ratio of time spend in the inner and outer ring is calculated. 1 signifies the fly has spent all its time in the outer part of the arena. −1 signifies the fly was at all times in the inner part of the arena. 0 would signifiy an equal distribution between inner and outer part of the arena: Only parts of the track while the fly is moving count to the calculation.
12. **Centrophobism while stationary:** Only parts of the track while the fly is not moving count to the calculation.
13. **Center deviation while moving:** Deviation away from the center of the platform. Values given in percent of the radius. Only parts of the track while the fly is moving count to the calculation.
14. **Center deviation while stationary:** Only parts of the track while the fly is not moving count to the calculation.

Measures of angles or location relative to visual cue

15. **Absolute angle deviation:** Deviation angle from the path a fly walks away from the direction of the closest stripe. Direction does not matter. Median of all deviations is reported in degrees.
16. **Stripe deviation while moving:** Deviation away from the idealized line through the middle of the stripe. Direction toward right or left does matter. Values given in percent of the radius
17. **Stripe deviation while stationary:** Deviation away from the idealized line through the middle of the stripe. Direction toward right or left does matter. Values given in percent of the radius.
18. **Absolute stripe deviation while moving**: Deviation away from the idealized line through the middle of the stripe. Direction toward right or left does not matter. Values given in percent of the radius.
19. **Absolute stripe deviation while stationary:** Deviation away from the idealized line through the middle of the stripe. Direction toward right or left does not matter. Values given in percent of the radius.
20. **Angle deviation while stationary:** Deviation away from the idealized line through the middle of the stripe. Direction toward right or left does not matter. Values given in percent of the radius.
21. **Angle deviation while moving:** Deviation angle from the path a fly walks away from the direction of the closest stripe. Direction does matter. Median of all deviations is reported in degrees.
22. **Horizon deviation while moving:** Deviation away from the idealized line perpendicular to the stripes. Direction toward top or bottom stripe does matter. Values given in percent of the radius.
23. **Horizon deviation while stationary:** Deviation away from the idealized line perpendicular to the stripes. Direction toward top or bottom stripe does matter. Values given in percent of the radius.
24. **Absolute horizon deviation while moving:** Deviation away from the idealized line perpendicular to the stripes. Direction toward top or bottom stripe does not matter. Values given in percent of the radius.
25. **Absolute horizon deviation while stationary:** Deviation away from the idealized line perpendicular to the stripes. Direction toward top or bottom stripe does not matter. Values given in percent of the radius.

The data was statistically analyzed using the Kruskal- WIlis rank sum test and pairwise Wilcoxon rank sum test as a post hoc test using R. (The post hoc test was corrected with the Benjamini-Hochberg procedure to correct for multiple comparison.)

Mathematical modeling

We adapted the data-driven stochastic model from Özel et al., 2019 by omitting the filopodia compartment and estimating temperature-specific parameters from the live imaging data (bulbous life time, number of bulbous tips at P60). In brief, we modeled synapses (S), short-lived transient bulbous tips (sB) and stable synaptogenic bulbous tips (synB).

The model's reaction stoichiometries are determined by the following reaction scheme:

$$R_1 : \emptyset \rightarrow sB, \quad R_2 : sB \rightarrow \emptyset, \quad R_3 : sB \rightarrow synB, \; R_4 : synB \rightarrow S + synB, \; R_5 : synB \rightarrow \emptyset$$

Reaction R_1 denotes the formation of a (transient) bulbous tip, while R_2 denotes its retraction. Reaction R_3 denotes the stabilization of a transient bulbous tip, a stable bulb forms a synapse with reaction R_4, while the bulbous tip remains visible and R_5 denotes the retraction of a stable bulb. Note that in R_1 we only implicitly model filopodia as outlined below.

Similar to the published model in Özel et al., 2019, reaction rates/propensities of the stochastic model are given by

$$r_1(t,B) = r_1(P60) \cdot f_1(synB, B_{50}) \cdot \frac{f_{FB}\left(t, t_{\frac{1}{2}}\right)}{f_{FB}\left(P60, t_{\frac{1}{2}}\right)} \cdot \frac{f_F(t)}{f_F(P60)},$$

$$r_2(sB) = c_2 \cdot sB,$$

$$r_3(sB) = c_3 \cdot sB,$$

$$r_4(synB) = c_4 \cdot synB,$$

$$r_5(synB) = c_5 \cdot synB$$

where $c_2, \ldots, c_5$ are reaction constants (estimated as outlined below). The feedback function $f_1(synB, B_{50}) = (synB + B_{50}) / B_{50}$ models bulbous auto-inhibition due to limited resources and synaptic seeding factor competition as introduced before (Özel et al., 2019) and $r_1(P60)$ denotes the *net rate* of emergence of bulbous tips at *developmental time* P60. We do not consider the emergence of bulbous tips from filopodia as in previous work[1], but rather implicitly through the time-dependent function $f_F(t)$. The functions $f_F(t)$ and $f_{FB}\left(t, t_{\frac{1}{2}}\right)$ model slow-scale dynamics of filopodia- and bulbous dynamics, with previously determined parameters (Özel et al., 2019):

$f_{FB}(t)$ is a tanh function with

$$f_{FB}(t, t_{1/2}) = \frac{1}{2}\left(1 + \tanh\left[\frac{3}{t_{1/2}}\left(t - t_{1/2}\right)\right]\right)$$

that models a time-dependent increase in the propensity to form bulbous tips with $t_{1/2}$ = 1000 (min). The time-dependent function $f_F(t) = \max(0, \sum_{i=0}^{5} p_i \cdot t^i)$ is a fifth-order polynome with coefficients $p_5 = -2.97 \cdot 10^{-14}$, $p_4 = 3.31 \cdot 10^{-13}$, $p_3 = -1.29 \cdot 10^{-9}$, $p_2 = 2.06 \cdot 10^{-6}$, $p_1 = -1.45 \cdot 10^{-3}$ and $p_0 = 1$ that downregulates the generation of new filopodia at a slow timescale. Note, that t denotes the time in (min) after P40 (e.g., $t_{P40} = 0$ and t_{P60} = 60*20*scaling factor), which is scaled according to the factors discussed in the section 'Developmental time adjustment below. The model was simulated using the Gillespie algorithm as outlined in (Özel et al., 2019).

'Developmental time' adjustment.

At 25°C, the pupal developmental stages correspond to the number of hours passed since pupation. For example, 'P60' refers to the pupal development stage observed at 60 hours past pupation at 25°C. For the different temperatures the pupal development stages correspond to different durations past pupation. We measured that at 18°C, the pupal development stage P100 is achieved 200.88 hours after pupation. At 29°C it is achieved after 88.08 hours. Thus, for the different temperatures there are distinct factors that relate *real time* to *pupal development stage* as shown here:

temp	developmental time P0 to P100 [hours]	factor
18°C	200.88	2.05
25°C	**98.16**	**1.00**
29°C	88.08	0.90

We used these scaling factors to relate *real time* to *developmental time* in our model simulations

Parameter estimation

Using the methods explained below, we derived the parameters as shown below.

We first investigated the lifetimes of bulbous tips (Figure 1F) and fitted parameter c_2 and c_5 which relates to the retraction of short- and long-lived bulbous tips, as shown in Figure S13.

We then estimated the three parameters $r_1(t = P60)$, c_3 and B_{50}. To do so, we used the number distribution of short-lived and synaptogenic bulbous tips and set up the generator matrix

$$G([i,j],[i-1,j]) = i \cdot c_2, \quad G([i,j],[i,j-1]) = j \cdot c_5$$

$$G([i,j],[i+1,j]) = r_1(P60) \cdot f_1(j, B_{50}), \quad G([i,j],[i,j+1]) = j \cdot c_3$$

with diagonal elements such that the row sum equals 0. In the notation above, the tupel [i, j] denotes the state where *i* short- lived bulbous tips *sB* and *j* synaptogenic bulbous tips *synB* are present. The generator above has a reflecting boundary at sufficiently large N (maximum number of bulbous tips). Above, $r_3(t)$ is auto-inhibited by the number of stable bulbous tips through function f_1. The stationary distribution of this model is derived by solving the eigenvalue problem

$$G^T \cdot v = v \cdot \lambda$$

and finding the eigenvector corresponding to eigenvalue $\lambda_0 = 0$. From this stationary distribution, we compute the marginal densities of *sB* and *synB* (e.g., summing over all states where i = 0, 1, ... for sB) and fit them to the experimentally derived frequencies by minimizing the Kullback-Leibler divergence between the experimental and model-predicted distributions. Estimated parameters $r_1(t = P60)$, c_3 and B_{50} are shown in the following table:

	r_1(P60)	B_{50}	c_2	c_3	c_4	c_5
18°C	0.3056	0.1187	0.0706	0.0427	0.0033	0.006
25°C	0.0860	0.3505	0.0706	0.0207	0.0091	0.006
29°C	0.0569	0.1044	0.0706	0.0081	0.0200	0.006

Finally, c_4 was determined based on measured synapse numbers at P100.

Cell Reports, Volume *37*

Supplemental information

Brain connectivity inversely scales with developmental temperature in *Drosophila*

Ferdi Ridvan Kiral, Suchetana B. Dutta, Gerit Arne Linneweber, Selina Hilgert, Caroline Poppa, Carsten Duch, Max von Kleist, Bassem A. Hassan, and P. Robin Hiesinger

Figure S1

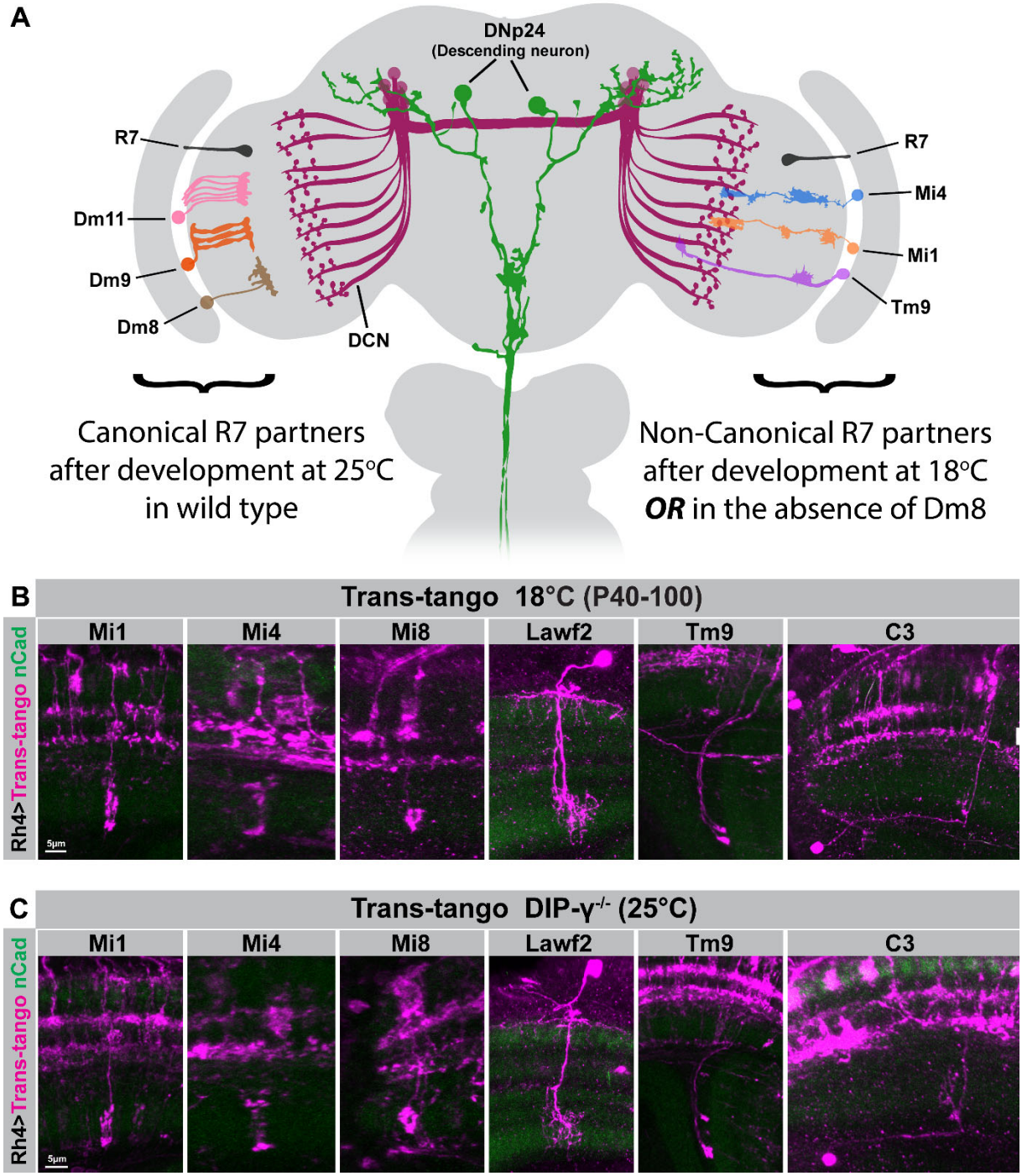

Figure S1. yR7s connect to the same types of non-canonical postsynaptic partners in wild type after development at 18°C and in DIPγ mutants after development at 25°C. Related to Figures 2 and 3.

(A) Schematic of neurons investigated in this study. The left side depicts canonical R7 partner neurons, the right side non-canonical R7 partners. **(B-C)** Representative images of neurons postsynaptically connected to yR7 photoreceptors in wild-type brains after development at 18°C **(B)** and in DIPγ mutant brains after development at 25°C **(C)**. Note that development at 18°C in wild type and at 25°C in the DIPγ mutant leads to non-canonical synaptic partnerships with the same type of neurons.

Figure S2

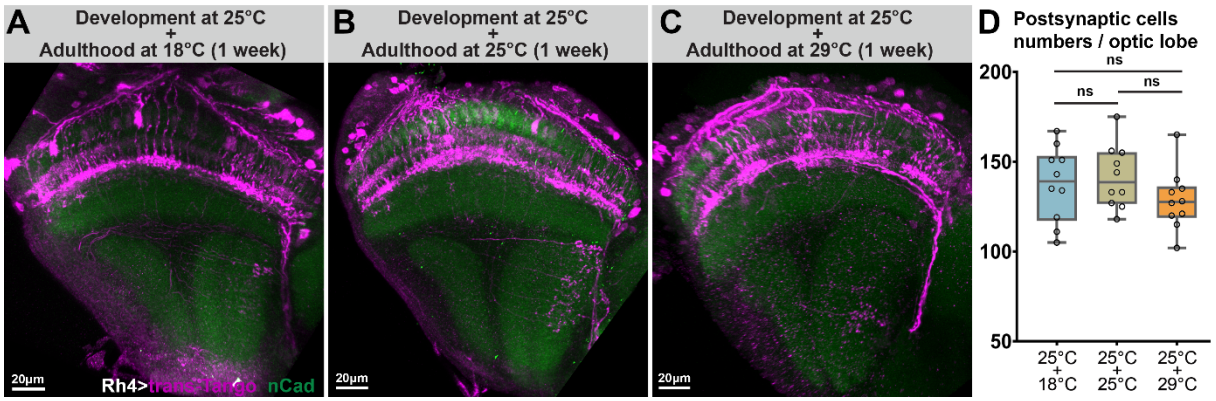

Figure S2. Alterations of temperature during the first week of life do not lead to differences in postsynaptically connected cell numbers. Related to Figure 2.

(A-C) Representative images of neurons postsynaptically connected to yR7 photoreceptors in brains developed at 25°C and then shift to either 18°C **(A)**, kept at 25°C **(B)** or shift to 29°C **(C)** during the first week of adult life prior to a trans-Tango experiments. **(D)** The number of neurons connected to yR7 photoreceptors do not significantly change when developed at the same temperature (25°C) and exposed to different 'functional' temperatures during adulthood. n=10 optic lobes (from 10 individual flies) per condition. Data was analyzed with the Kruskal-Wallis test and Dunn's as post-hoc test; ns=not significant.

Figure S3

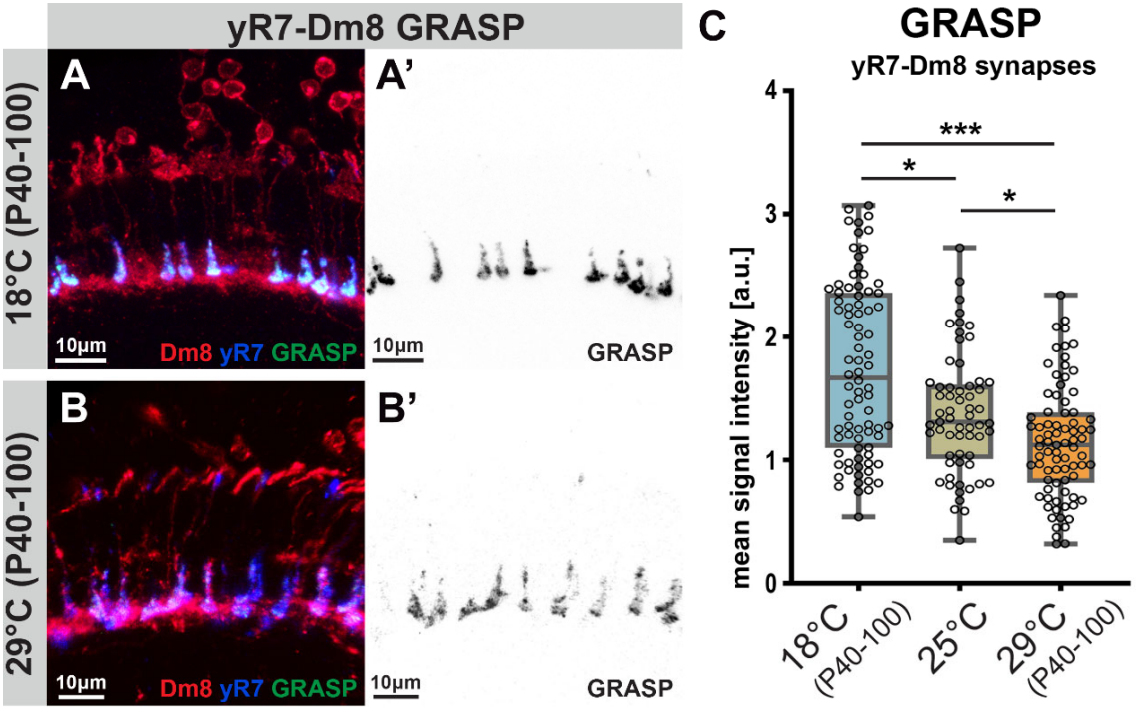

Figure S3. Activity-dependent GRASP labeling of yR7s and their main synaptic partner Dm8s scales with developmental temperature. Related to Figure 2.

(A-B') Representative images of activity-dependent GRASP between yR7s and Dm8 after development at 18°C **(A-A')** and after development at 29°C **(B-B')**. **(C)** Low developmental temperature scales with the GRASP signal between yR7s and their main synaptic partner Dm8. n=85 terminals, 13 flies per condition. Data was analyzed with the Kruskal-Wallis test and Dunn's as post-hoc test; *p<0.0332, ***p<0.0002.

Figure S4

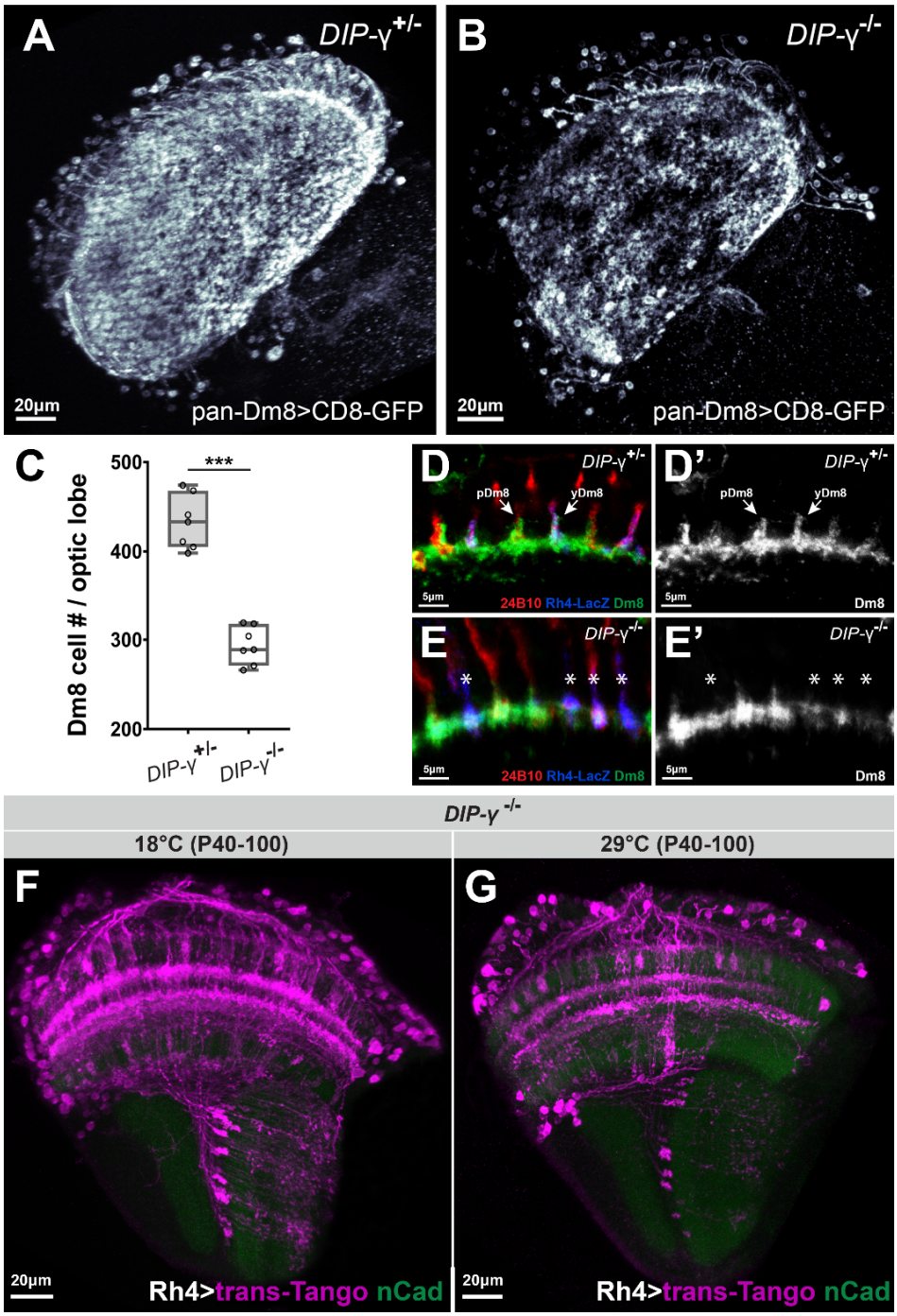

Figure S4. Loss of the majority of DIPγ⁺Dm8 neurons leads to increased recruitment of non-canonical synapses of yR7 neurons. Related to Figure 3.

(A-C) DIPγ loss-of-function leads to cell death of the majority of DIPγ⁺Dm8 neurons. n=7 optic lobes (from 7 individual flies) per condition. **(D-E)** Surviving DIPγ⁺Dm8 neurons lack distal membrane protrusions at medulla layers M4-M5. **(F-G)** Non-canonical partner neurons (Mi cells, C2/C3 cells, and Tm9) in DIPγ mutant brains scale with developmental temperatures of 18°C **(F)** and 29°C **(G)**, revealing an additive effect of low developmental temperature andmain synaptic partner loss on partner availability. Data was analyzed with the Kolmogorov-Smirnov test; ***p<0.0002.

Figure S5

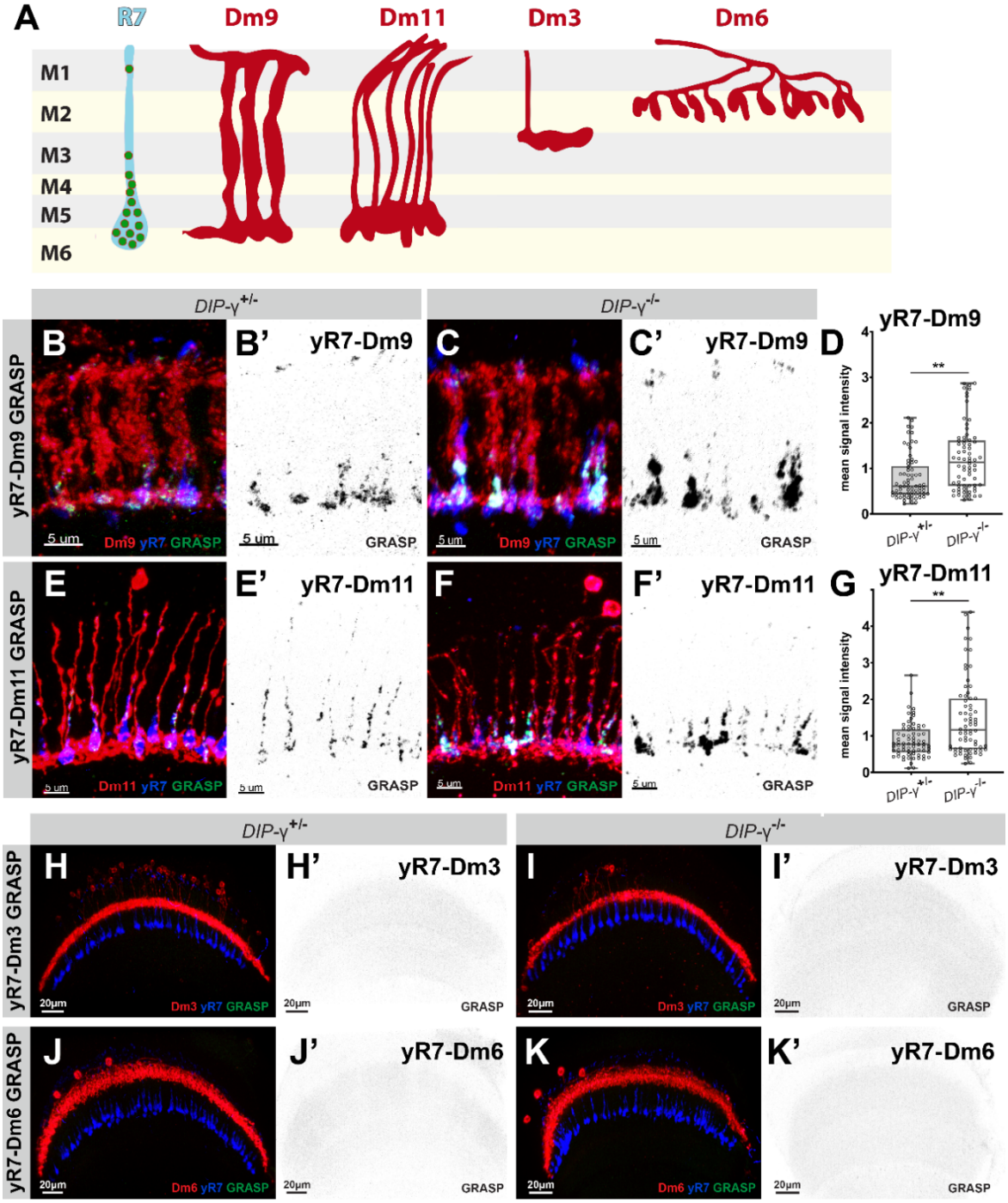

Figure S5. Loss of the majority of DIPγ⁺Dm8 neurons leads to increased activity-dependent GRASP signals of yR7 with canonical synaptic partners Dm9 and Dm11. Related to Figure 3.

(A) Schematic representations of Dm9, Dm11, Dm6, and Dm3 neurons with an R7 terminal through medulla layers M1-M6. Green dots demonstrate the distribution of active zones in R7 terminals based on the connectome data. **(B-G)** Activity-dependent GRASP between yR7s and Dm9 **(B-D)** and between yR7s and Dm11 **(E-G)** in control and DIPγ mutant brains reveals stronger synaptic connections with the loss of main synaptic partner Dm8. n=70-80 terminals, 10-12 flies per condition. **(H-K')** Dm8 neuron loss in DIPγ mutants does not lead to synapse formation with neurons (Dm3 and Dm6) that do not have dendritic branches in medulla layers. Data was analyzed with the Kolmogorov-Smirnov test; **p<0.0021.

Figure S6

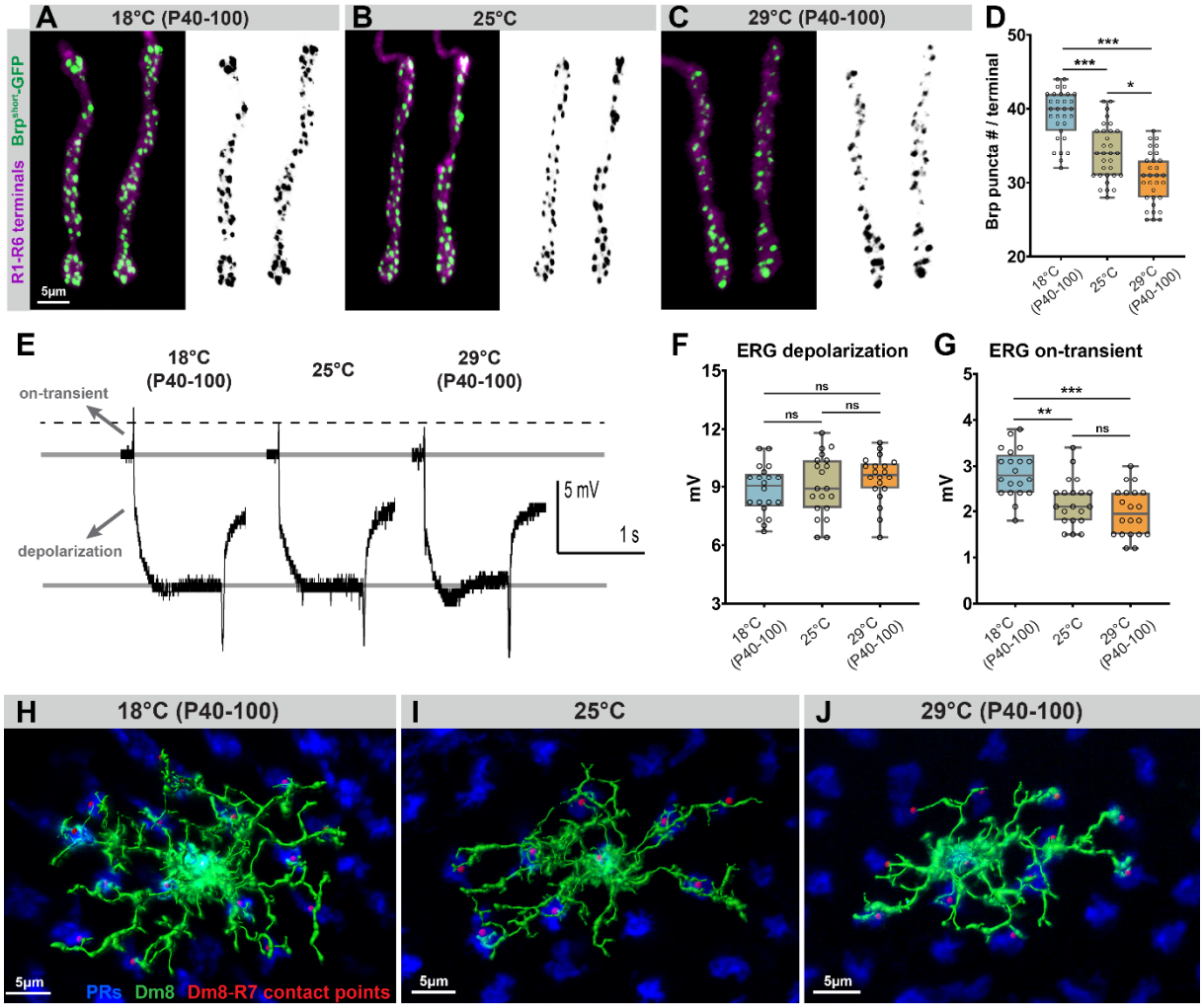

Figure S6. R1-R6 photoreceptor synapse number and neurotransmission as well as Dm8 arborizations scale with developmental temperature. Related to Figure 4.

(A-C) Representative images of R1-R6 photoreceptor axon terminals with GFP-BrpD3 (Brp^{short}) marked active zones developed at 18°C **(A)**, 25°C **(B)**, and 29°C **(C)**. **(D)** The number of active zones per R1-R6 terminal at different developmental temperatures. n=30 terminals, 6 flies per condition. **(E)** Representative electroretinogram (ERG) traces recorded from fly eyes developed at 18°C, 25°C, and 29°C. **(F)** Developmental temperature does not affect phototransduction based on ERG 'depolarization' amplitudes. n=20 flies per condition. **(G)** Low developmental temperature increases neurotransmission of R1-R6 photoreceptors based on ERG 'on-transient' amplitudes. n=20 flies per condition. Data was analyzed with the Kruskal-Wallis test and Dunn's as post-hoc test; *p<0.0332, **p<0.0021, ***p<0.0002, ns=not significant. **(H-J)** Skeleton reconstructions of Dm8 cells developed at 18°C **(A)**, 25°C **(B)**, and 29°C **(C)**.

Figure S7

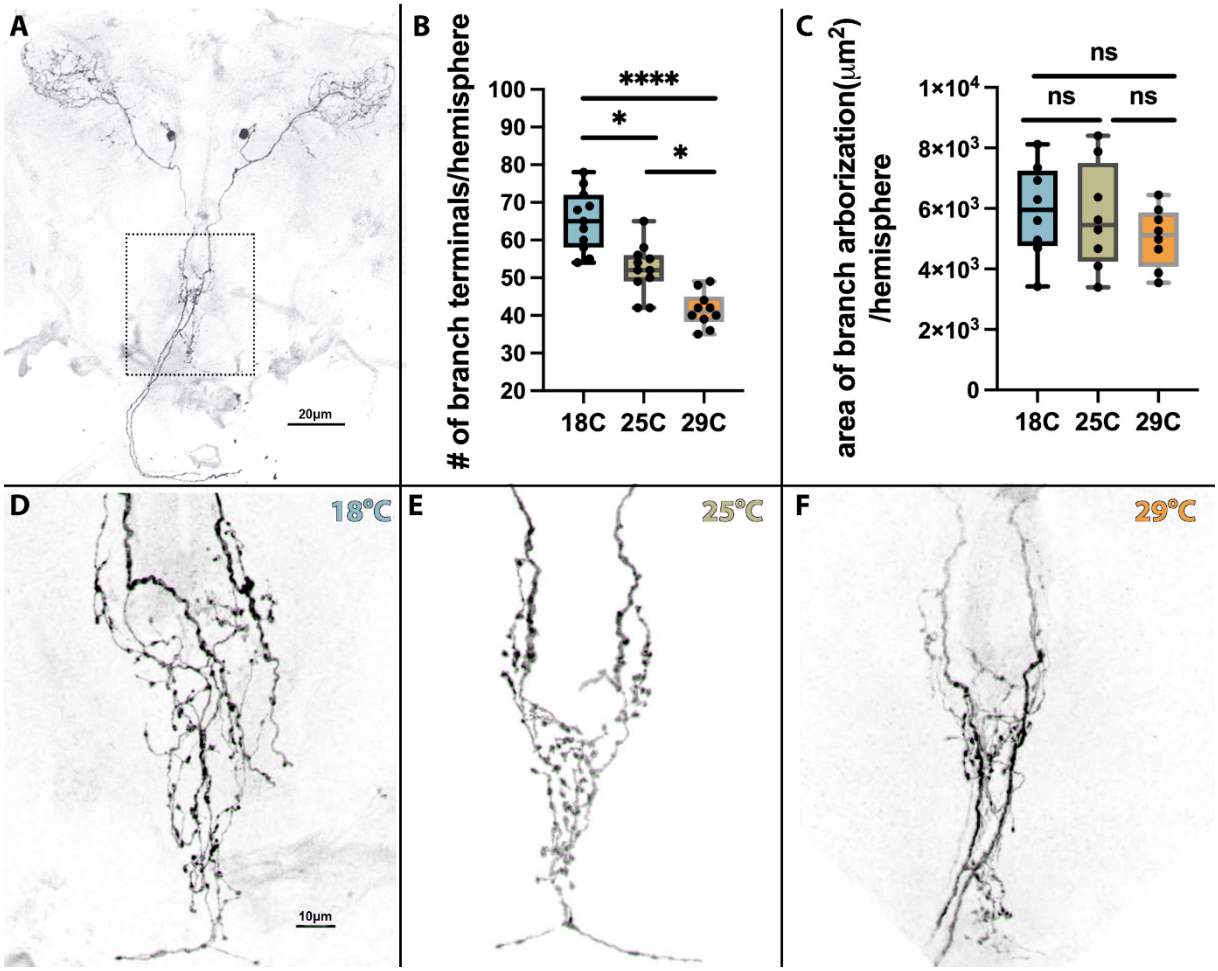

Figure S7. The descending neurons DNp24 exhibits temperature-dependent branch numbers, but temperature-independent areas of branch coverage. Related to Figure 4.

(A) Expression of the Janelie SS00732 split-Gal4 line. **(B-C)** quantification of axonal branches shown in the boxed region in **(A).** **(D-F)** representative pictures of the axonal branches after developmental at three different temperatures.

Figure S8

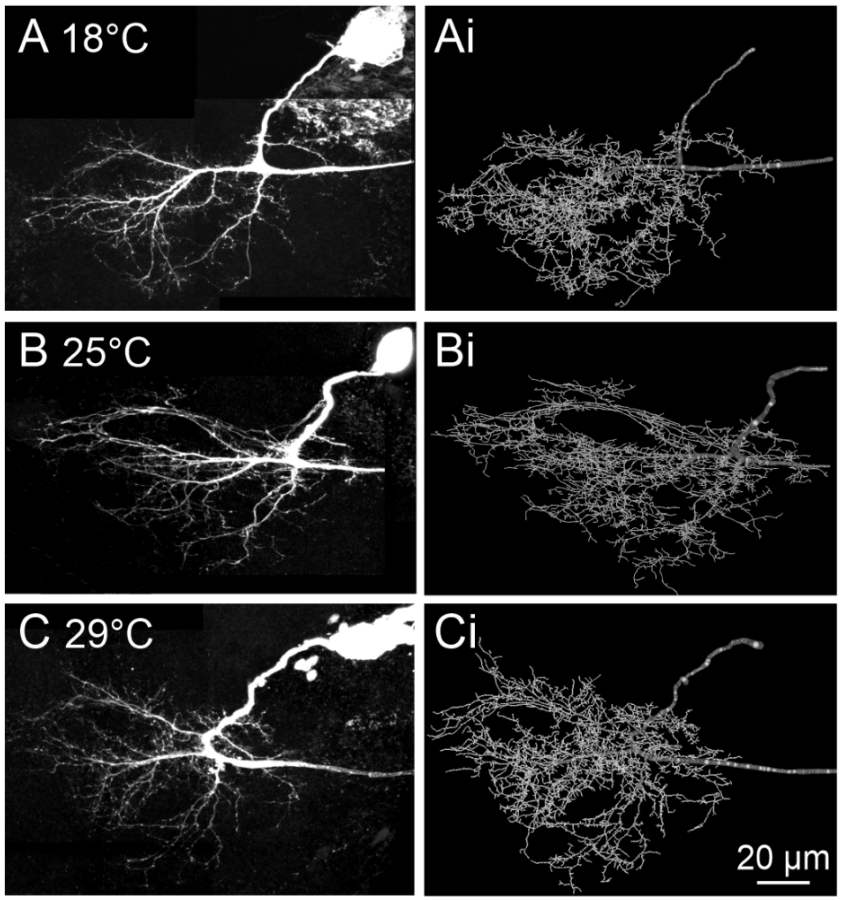

D morphometry

	18° C	25° C	29° C
branch # [n]	3131	3097	3043
TDL [µm]	5420	6360	5275
MDL [µm]	1.74	2.06	1.74
MDR [µm]	0.24	0.23	0.23

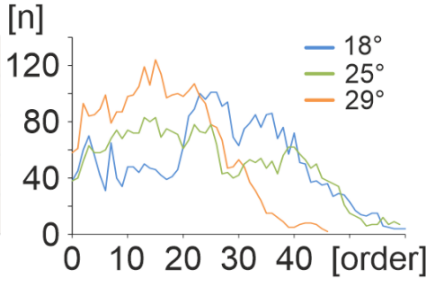

Figure S8. Developmental temperature does not affect motoneuron dendritic branch number but branch organization. Related to Figure 4.

(A-C) Maximum intensity projection views from confocal image stacks of representative adult DLM motoneurons filled intracellularly after pupal development at 18°C **(C)**, 25°C **(B)**, and 29°C **(C)**. **(Ai-Ci)** 3D geometric reconstructions of the motoneuron dendrites shown in A-C. **(D)**. The number of branches, total dendritic length (TDL), the mean length of all dendritic branches in a reconstruction (MDL), and the mean radius of all dendritic branches (MDR) for 18°C (blue), 25°C (green), and 29°C (orange). **(E)** For each temperature the number of dendritic branches is plotted over the branch order in which these branches occur. The primary neurite connecting the soma and the axon was defined as tree origin, and thus branch order 0. Any dendrite branching off the origin is branch order 1, any dendrite branching off order n is defined as order n+1.

Figure S9

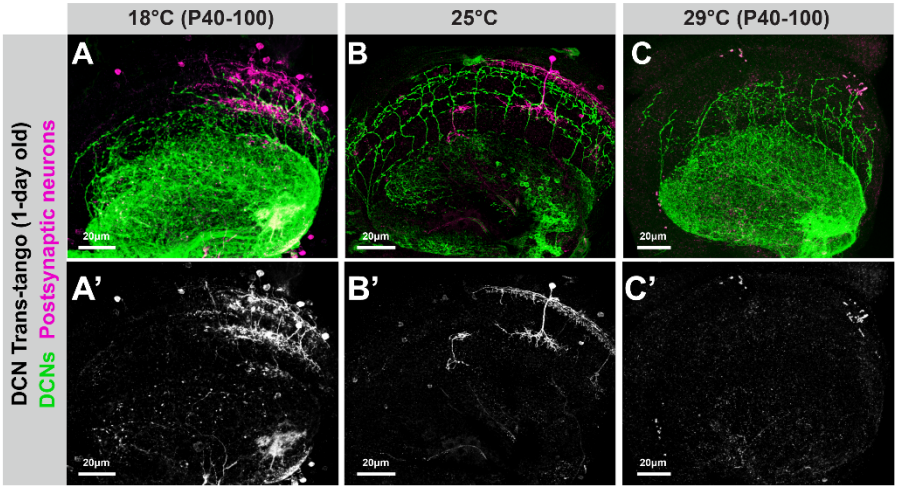

D

Postsynaptic cell # /optic lobe

Cell type	18°C (P40-100)	25°C
Lawf1/2	7,15±1,74	1,12±0,31
L cells	0,38±0,38	0
Lpi	0,07±0,07	0

Figure S9. Branch elaboration and partner availability of DCNs scale with developmental temperature. Related to Figures 4 and 5.

(A-C) Low developmental temperature leads to more widespread labeling of neurons postsynaptically connected to DCNs. **(D)** rarely connected cell types (L cells and Lpi cells) were only observed when brains developed at 18°C. n=8 optic lobes (from 8 individual flies) per condition.

Supplementary Figure S10 - Behavioral Temperature 25°C

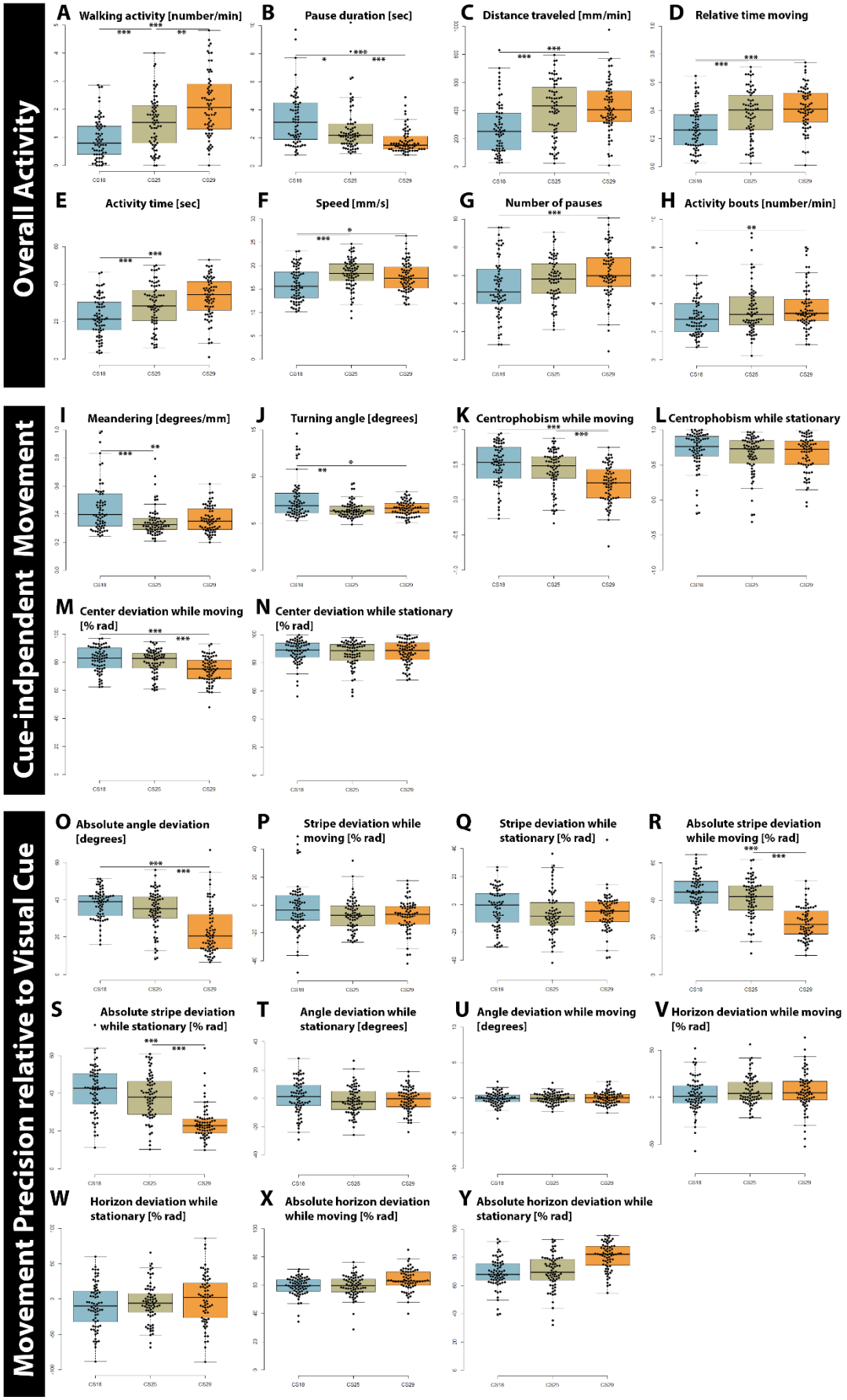

Figure S10. Analysis of 25 behavioral parameters in Buridan's paradigm at a behavioral emperature of 25°C. Related to Figure 6.

(A-H) Most parameters related to overall activity of flies in Buridan arena increase after development at high temperatures. **(I-Y)** Parameters related to cue-dependent and cue-independent movement precision are largely temperature-compensated. n=70 flies per condition. See Table S3 for quantifications.

Supplementary Figure S11 - Behavioral Temperature 18°C

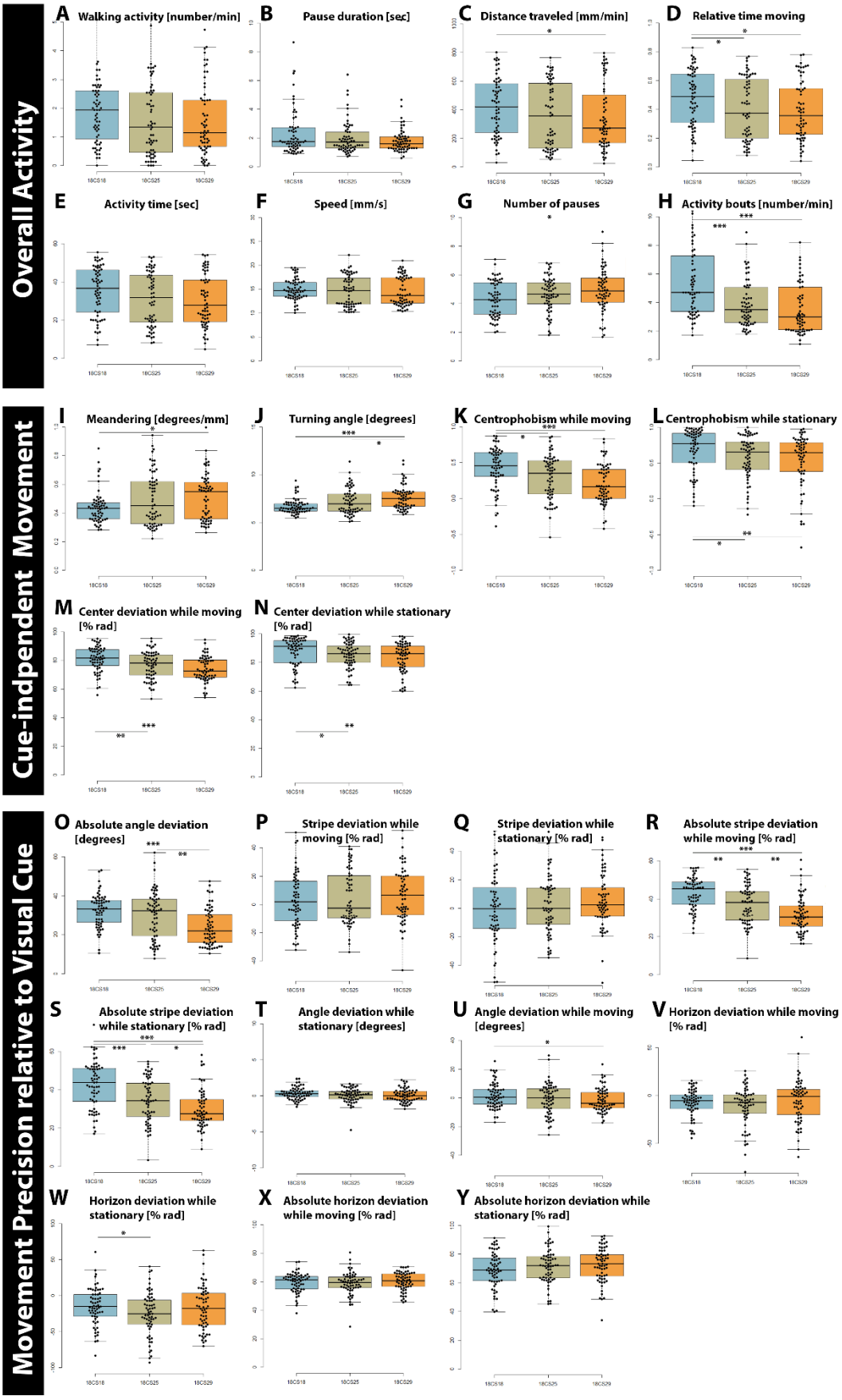

Figure S11. Analysis of 25 behavioral parameters in Buridan's paradigm at a behavioral emperature of 18°C. Related to Figure 6.

(A-H) Most parameters related to overall activity of flies in Buridan arena increase after development at high temperatures. **(I-Y)** Parameters related to cue-dependent and cue-independent movement precision are largely temperature-compensated. n=70 flies per condition.

Supplementary Figure S12 - Behavioral Temperature 29°C

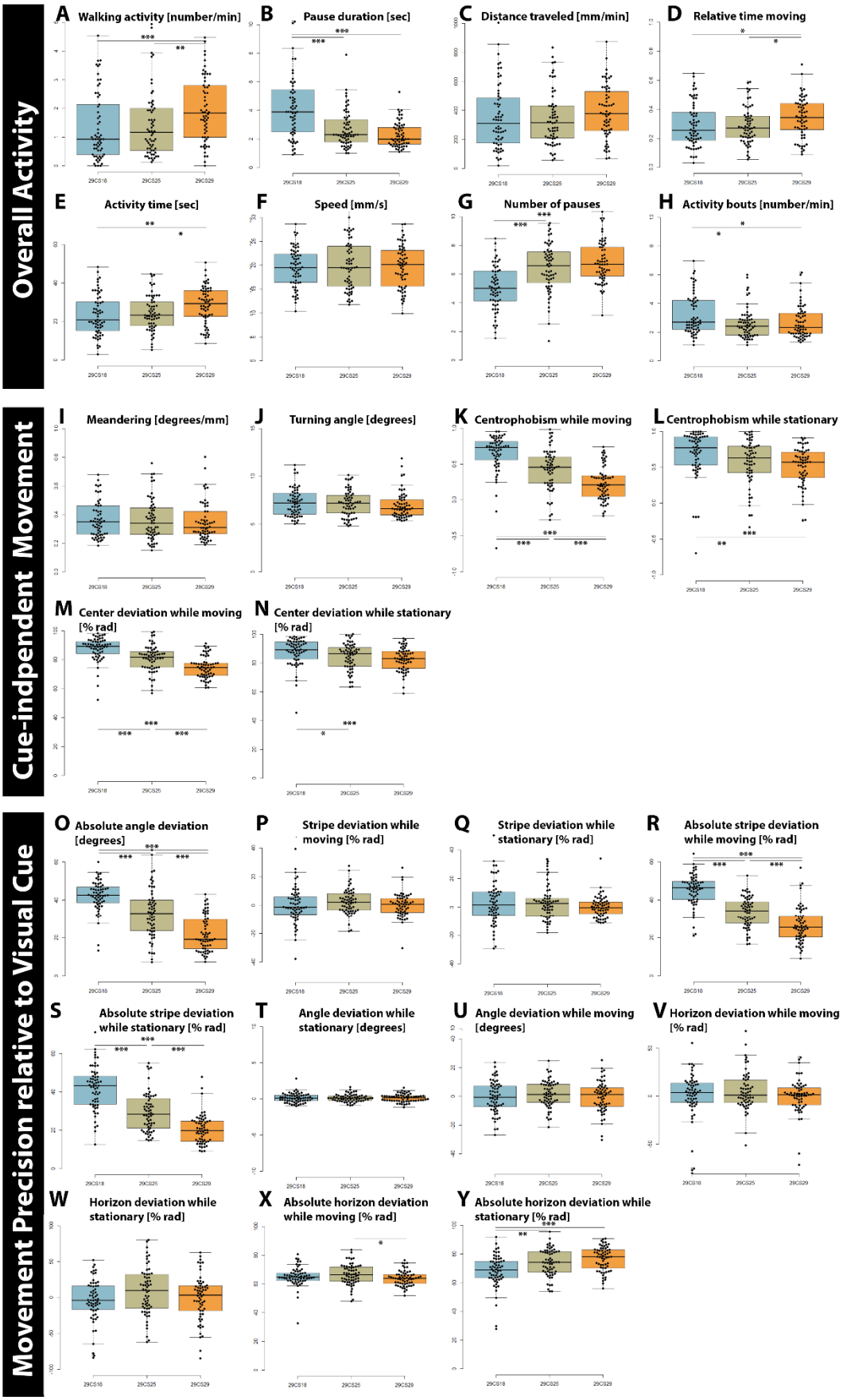

Figure S12. Analysis of 25 behavioral parameters in Buridan's paradigm at a behavioral emperature of 29°C. Related to Figure 6.

(A-H) Most parameters related to overall activity of flies in Buridan arena increase after development at high temperatures. **(I-Y)** Parameters related to cue-dependent and cue-independent movement precision are largely temperature-compensated. n=70 flies per condition.

Figure S13

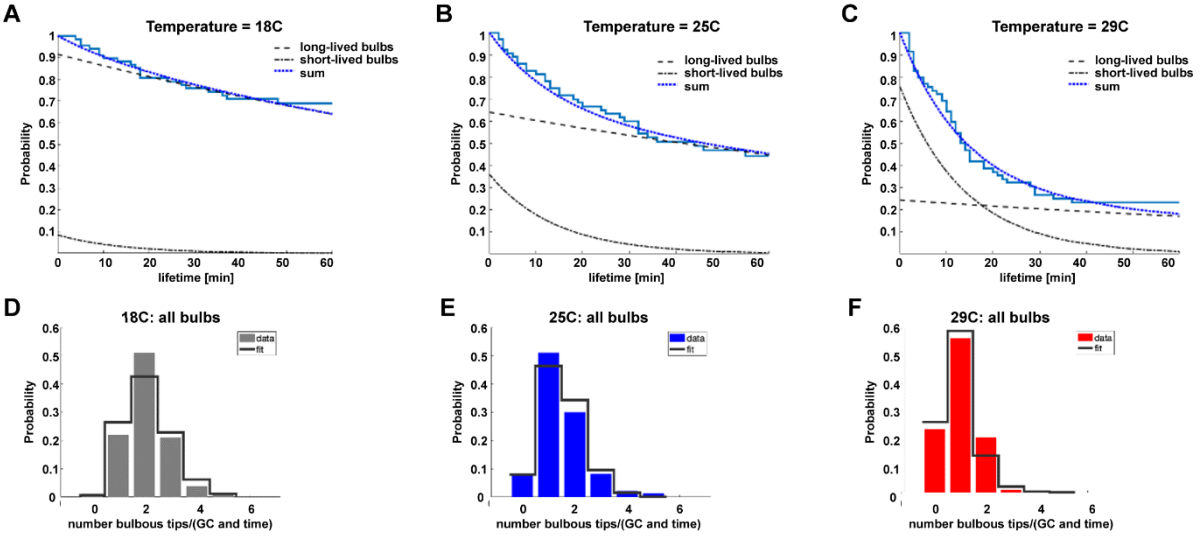

Figure S13. Quantitative analyses of R7 bulbous tips (synaptigenic filopodia) lifetimes and numbers. Related to STAR Methods.

(A-C) Data derived (solid blue stairs) and fitted (continuous dotted blue line) bulbous lifetime kinetics. We assumed that the life time kinetics are resulting from the combined kinetics of short-lived and synaptogenic bulbous tips (black dotted and dashed lines). Fitted parameters: $c_2 = 0.0706\ min^{-1}$; retraction rate of the synpatogenic bulbous tips was estimated to be $c_5 = 0.006\ min^{-1}$ and the proportion of synaptogenic bulbous tips was 0.92, 0.64 and 0.24 at 18, 25 and 29°C. **(D-F)** Data derived (bars) and fitted (solid line) number distribution for bulbous tips at developmental stage P60 for 18, 25 and 29°C.

	18	sem	25	sem	29	sem	25/18	29/18	29/25
R7 Filopodia speed (um/min)	**0,827**	0,058	**1,155**	0,072	**1,472**	0,079	**1,396614**	1,779927	1,274459
R7 Filopodia Lifetime (min)	**10,088**	0,807	**6,638**	0,627	**4,3**	0,429	**1,519735**	2,346047	1,543721
R7 BrpD3 active zones (#/terminal)	**24,65**	0,523	**20,65**	0,323	**16,35**	0,597	**1,193705**	1,507645	1,262997
R7 trans-Tango (# cell/optic lobe)	**183,7**	7,106	**145,3**	7,027	**133,8**	6,335	**1,264281**	1,372945	1,085949
R7-Dm8 GRASP (mean signal int.)	**0,17**	0,008	**0,137**	0,006	**0,116**	0,005	**1,240876**	1,465517	1,181034
R7-Dm9 GRASP (mean signal int.)	**0,093**	0,009	**0,066**	0,006	**n/a**	n/a	**1,409091**	n/a	n/a
R7-Dm11 GRASP (mean signal int.)	**0,115**	0,011543	**0,079**	0,003	**n/a**	n/a	**1,455696**	n/a	n/a
DCN Filopodia speed (um/min)	**0,235738736**	0,01946	**0,372921847**	0,031406	**0,761213**	0,105939	**1,581929**	3,229053	2,041213
DCN primary branch number	**7,074074074**	0,417336	**5,227272727**	0,40649	**2,62069**	0,209537	**1,353301**	2,699318	1,994617
DCN secondary branch number	**3,676470588**	0,54257	**1,484848485**	0,267191	**0,489796**	0,115911	**2,47599**	7,506127	3,031566
DCN BrpD3 active zones (#/terminal)	**0,275**	0,008	**0,241**	0,009	**0,104**	0,01	**1,141079**	2,644231	2,317308
DCN trans-Tango (# cells/optic lobe)	**88,83**	9,964	**55**	2,637	**13**	2,65	**1,615091**	6,833077	4,230769
DCN-Lawf1 GRASP (mean signal int.)	**0,259354806**	0,009516	**0,173174065**	0,00545	**n/a**	n/a	**1,497654**	n/a	n/a
R1-6 BrpD3 active zones (#/terminal)	**39,223**	0,595	**34,097**	0,668	**30,548**	0,637	**1,150336**	1,283979	1,116178
R1-6 ERG on transient (mV)	**2,85**	0,118433	**2,205**	0,114817	**1,985**	0,118383	**1,292517**	1,435768	1,110831
R1-6 ERG depolarization (mV)	**8,855**	0,283445	**9,095**	0,356996	**9,46**	0,273515	**0,973612**	0,936047	0,961416
Dm8 branch numbers	**321,28**	14,4	**259,94**	11,29	**215,87**	8,35	**1,235978**	1,488303	1,204151
Dm8 total branch length	**505,5074801**	25,38734	**429,0747891**	20,30404	**328,7044**	16,81363	**1,178134**	1,537878	1,305351
Dm8 overlap with #R7s	**14,73333333**	0,693278	**11,76470588**	0,525311	**10,23529**	0,565747	**1,252333**	1,439464	1,149425
Mi4 branch numbers	**284,12**	9,06	**246,43**	8,93	**197**	6,14	**1,152944**	1,442234	1,250914
Mi4 total branch length	**397,4117872**	12,90929	**349,6517454**	11,07318	**274,7308**	7,369114	**1,136593**	1,44655	1,272707

Table S1. Related to Figures 1, 2, 3, 4, and 5. Summary of quantitative analyses of temperature effects in wild type.

	DIP γ control	sem	DIPγ null	sem	DIPγ null/control
R7-Dm8 GRASP (mean signal int.)	**0,12866698**	0,010655	**0,074990253**	0,007825	**0,58282438**
R7-Dm9 GRASP (mean signal int.)	**0,07956988**	0,005975	**0,122924772**	0,00872	**1,544865632**
R7-Dm11 GRASP (mean signal int.)	**0,087511903**	0,005743	**0,147890694**	0,012554	**1,689949474**
R7-Mi1 GRASP (mean signal int.)	**0,008177834**	0,000401	**0,080416746**	0,005984	**9,833502068**
R7-Mi4 GRASP (mean signal int.)	**0,007972476**	0,000409	**0,045601459**	0,003249	**5,719861385**
R7-Tm9 GRASP (mean signal int.)	**0,006905958**	0,000597	**0,041563339**	0,002742	**6,018475543**

Table S2. Related to Figure 3. Summary of quantitative analyses of temperature effects in DIPγ mutants.

	25/18	29/18	29/25	
Walking activity	**1,597938144**	**2,278350515**	**1,425806452**	Temperature-Dependent
Pause duration	**1,541818182**	**2,141414141**	**1,388888889**	
Distance traveled	**1,505164492**	**1,560668995**	n.s.	
Relative time moving	**1,407407407**	**1,518518519**	n.s.	
Meandering	**1,351351351**	**1,388888889**	n.s.	
Activity time	**1,311461067**	**1,46544182**	n.s.	
Turning angle	**1,178678679**	**1,193009119**	n.s.	
Speed	**1,143125**	**1,09875**	n.s.	
Number of pauses	n.s. (p=0.053)	**1,202312139**	n.s. (p=0.06)	
Activity bouts	n.s.	**1,179245283**	n.s.	
Centrophobism while moving	n.s.	**2,272727273**	**1,909090909**	
Absolute stripe deviation while moving	n.s.	**1,718685832**	**1,566735113**	
Absolute stripe Deviation while stationary	n.s.	**1,605501267**	**1,491132827**	
Absolute angle Deviation	n.s.	**1,595699831**	**1,452782462**	
Absolute horizon deviation while stationary	n.s.	n.s.	**1,154741379**	
Absolute horizon deviation while moving	n.s.	n.s.	**1,071260504**	
Center deviation while moving	n.s.	n.s.	**0,931900537**	
Stripe deviation while stationary	n.s. (p=0.051)	n.s.	n.s.	Temperature-Compensated
Stripe deviation while moving	n.s. (p=0.057)	n.s.	n.s.	
Angle deviation while stationary	n.s.	n.s.	n.s. (p=0.054)	
Centrophobism while stationary	n.s.	n.s.	n.s.	
Horizon deviation while stationary	n.s.	n.s.	n.s.	
Center deviation while stationary	n.s.	n.s.	n.s.	
Angle deviation while moving	n.s.	n.s.	n.s.	
Horizon deviation while moving	n.s.	n.s.	n.s.	

overall activity
movement angles or location independent of visual cue
movement angles or location relative to visual cue

Table S3. Related to Figure 6. Summary of quantitative analyses of behavioral parameters.